Journal of Seismology -PREPRINT

Deformation and Stress regimes in the Hellenic subduction zone from Focal Mechanisms

Marco Bohnhoff [1,*], Hans-Peter Harjes[2] and Thomas Meier[2]
[1] GeoForschungsZentrum Potsdam, 14473 Potsdam, Germany
[2] Faculty of Geosciences, Ruhr-University of Bochum, 44780 Bochum, Germany
*Corresponding author: email: bohnhoff@gfz-potsdam.de

Abstract

Fault plane solutions for earthquakes in the central Hellenic arc are analysed to determine the deformation and stress regimes in the Hellenic subduction zone in the vicinity of Crete. Fault mechanisms for earthquakes recorded by various networks or contained in global catalogues are collected. In addition, 34 fault plane solutions are determined for events recorded by our own local temporary network on central Crete in 2000-2001. The entire data set of 264 source mechanisms is examined for types of faulting and spatial clustering of mechanisms. Eight regions with significantly varying characteristic types of faulting are identified of which the upper (Aegean) plate includes four. Three regions contain interplate seismicity along the Hellenic arc from west to east and all events below are identified to occur within the subducting African lithosphere. We perform stress tensor inversion to each of the subsets in order to determine the stress field. Results indicate a uniform N-NNE direction of relative plate motion between the Ionian Sea and Rhodes resulting in orthogonal convergence in the western forearc and oblique (40-50°) subduction in the eastern forearc. There, the plate boundary migrates towards the SE resulting in left-lateral strike-slip faulting that extends to onshore Eastern Crete. N110°E trending normal faulting in the Aegean plate at this part is in accordance with this model. Along-arc extension is observed on Western Crete. Fault plane solutions for earthquakes within the dipping African lithosphere indicate that slab pull is the dominant force within the subduction process and interpreted to be responsible for the roll-back of the Hellenic subduction zone.

Keywords: Crete, Hellenic subduction zone, fault plane solutions, seismotectonics, deformation regime, stress tensor inversion

1. Introduction

The Hellenic subduction zone is the seismically most active region in Europe. There, the convergent plate boundary between the African lithosphere and the Aegean plate as part of Eurasia is located south of Crete in the Libyan Sea. It approaches the passive continental margin of northern Africa due to roll back of the Hellenic subduction zone and the convergence between Africa and Eurasia (e.g. McKenzie, 1970; LePichon and Angelier, 1979; Jackson and McKenzie, 1988; LePichon et al., 1995). The overall rate of convergence is 3-4 cm/year (e.g. McClusky et al., 2000). A well-developed Benioff zone was identified by seismicity to a depth of 150-180 km below the central Aegean (e.g. Papazachos, 1973; Makropoulos and Burton, 1981; Papadopoulos et al., 1986; Knapmeyer, 1999; Papazachos et al., 2000) and the subducting lithosphere can be followed down to about 1200 km by seismic tomography (e.g. Spakman et al., 1988; Bijwaard and Spakman, 1998). A tectonic reorganization in the entire south Aegean region at 3.4 Ma may mark the onset of continent-continent collision between the Aegean plate and the continental African plate (Lyon-Caen et al., 1988; LePichon et al., 1995: Mascle et al., 1999) at the western Hellenic arc. This resulted in a complex tectonic frame with a number of details such as the rapid uplift of western Crete (e.g. Lambeck, 1995) that are not yet fully understood. At the central and eastern part of the forearc indications for remnants of oceanic crust were identified (Bohnhoff et al., 2001; Brönner, 2003; Meier et al., 2004a).

Figure 1 gives an overview on the tectonic setting of the Aegean-Anatolian region with the Hellenic subduction zone. The island of Crete forms the central part of the Hellenic arc. Below the Libyan Sea an accretionary wedge with a sedimentary cover of up to 15 km is located between the active and passive continental margins. Recent microseismicity and surface wave studies (Meier et al., 2004b) as well as active seismic lines (Truffert et al., 1993; Bohnhoff et al., 2001; Brönner, 2003) allowed to refine the structural model along the Hellenic subduction zone (see inset in Figure 1) exemplifying the complex geometry along a strongly curved plate boundary.
The overall seismic activity of the Hellenic subduction zone is small compared to other subduction zones as can be observed from global earthquake catalogues. The distribution of hypocenters in the south Aegean region dominantly follows the Hellenic arc with stronger seismic activity observed in the eastern part. The hypocenters form an amphitheatrically shape of the Benioff zone in first order approximation (see e.g. Bath, 1983; Engdahl et al., 1998; Knapmeyer, 1999; Papazachos et al., 2000) and thus the trend of the steepest descent of the dipping slab significantly varies along the Hellenic arc. In contrast, the GPS horizontal velocities in this region as determined by McClusky et al. (2000) show only minor variation in trend (up to 18°) and magnitude (in the order of mm/a).
Several authors have analysed the stress field at the Hellenic subduction zone mainly based on fault trends and outcropping faults (e.g. Angelier et al., 1982; Meulenkamp et al., 1988; Ten Veen and Kleinspehn, 2003) or analysis of large earthquakes (Taymaz et al., 1990; Papazachos et al., 2000). In this study, we analyse fault mechanisms for earthquakes covering a broad magnitude range along the Hellenic arc in the vicinity of Crete. The area of investigation is indicated by the rectangle in Figure 1. We attempt to determine the deformation and stress regimes based on fault plane solutions that were collected from various local and regional studies as well as global catalogues. Furthermore, we newly determined fault plane solutions for smaller events recorded by our own local network in the Messara plain (Central Crete).

2. Data base and procedure applied

To compile a complete data base of fault mechanisms available we collected data from various published studies as well as from global catalogues available through the World Wide Web. We restricted the data base to events within 22.5-27.5°E and 33.5-36.5°N with no depth limitation. This resulted in a total of 352 events (including multiple occurrences) that cover a magnitude range between 0 and 6.5. Table 1 gives an overview on all events with occurrence time, hypocentral coordinates, magnitude, fault mechanisms and information on the relevant source. The sources that contributed to the data base and number of fault plane solutions taken are: Becker, 2000 [37 fault plane solutions]; Benetatos et al., 2004 [11], DeChabalier et al., 1992 [16]; Delibasis et al., 1999 [29]; Hatzfeld et al., 1993a and 1993b [37]; Jost et al., 2002 [12]; Kiratzi and Louvari, 2003 [8]; McKenzie, 1972 and 1978 [7]; Papadimitriou, 1993 [3]; Papadopoulos et al., 1986 [21]; Papazachos, 1973, Papazachos and Papazachou, 1997, Papazachos et al., 1991 and 2000 [24]; Taymaz et al., 1990 [14]; Harvard CMT, http://www.seismology.harvard.edu/CMTsearch.html, 1977-2004 [42]; MEDNET INGV, http://mednet.ingv.it/events/QRCMT/Welcome.html, 2001-2004 [10]; SED ETH Zürich, http://www.seismo.ethz.ch/mt, 2000-2004 [43]; USGS (except CMT solutions), http://neic.usgs.gov/neis/sopar, 1982-2002 [4]. Clearly, this catalogue is heterogeneous as it contains recordings from local, regional and global networks covering different time intervals as well as some relocations and redeterminations. Furthermore, non-uniform methods were used to determine the fault plane solutions (for description of methods used to determine the fault plane solutions in the individual studies we refer to the relevant article or webpage). Only some authors (Taymaz et al., 1990; Benetatos et al., 2004) give information on the accuracy of their fault mechanisms which was considered when skipping multiple-occurring events (see below). However, we assume having good control on the error bounds as we can compare the solutions from different sources for the same event in a number of cases. We thus estimate the overall errors for strike, dip and rake to be 15°. This value needs to be considered when discussing the significance of our results later in the text.
Some earthquakes occur plurally in Table 1 as they are listed in more than one study or catalogue and in some cases non-uniform fault mechanisms were given to the same event. We therefore carefully studied the entire catalogue and skipped multiple occurrences of individual earthquakes by eliminating all but the most reliable solution. We define the most reliable solution as the one determined with the best station configuration and most advanced method (which was usually that based on regional waveform modelling). This procedure reduced the catalogue to 232 fault mechanisms.

In addition to the collected fault plane solutions we determined source mechanisms for selected mircoearthquakes that were recorded by our own local network in southern central Crete in 2000/2001 (see Meier et al., 2004b). The network consisted of eight stations surrounding the Messara plain (see Figure 2, lower left). All stations were equipped with MARK 3C-L4 seismometers and operated at a 50 Hz sampling rate. Recordings from nearby permanent stations of the GEOFON network (Hanka and Kind, 1994) were added to improve the focal coverage for local events. To determine the source mechanisms we applied the FOCMEC program (Snoke et al., 1984; Snoke, 2003) that performs a grid-search assuming a pure double-couple mechanism. P wave polarities as well as SH/P amplitude ratios served as input data. To allow confident fault plane solutions we selected only events that occurred within or near the network and skipped those with errors >15°. This resulted in a total of 34 fault plane solutions covering a magnitude range from 0.3-3.5. Three examples of fault plane solutions and the station distribution of the seismic network in central Crete are shown in Figure 2.
Finally, the entire data set of fault mechanisms for earthquakes along the central Hellenic arc consists of 264 fault plane solutions that form the base for further analysis. Figure 3a shows the entire catalogue of fault plane solutions in a map view of the lower hemispheres. To further analyse the data base we focus on the orientations of maximum compression (P) and tension (T) in the following. In Figure 3b we plotted the P and T axes of the entire catalogue in an equal-area projection of the lower hemisphere and scaled the size and shading of circles with magnitude and hypocentral depth, respectively. The distribution of P and T axes indicates that the stronger and deeper events show preferred orientations whereas the smaller and shallower events indicate a comparatively high diversity of mechanisms. The magnitude frequency of all earthquakes is shown in Figure 4. The catalogue is complete for magnitudes ≥ 5. The large number of smaller ($M<3$) events documents the contributions from local networks on Crete that were operated for several (3-18) months. A remarkable decrease of number of events is observed within the range $3<M<5$. We explain this by the fact that such events are not recorded by the permanent global network (which allows completeness of $M=4$ only since the middle 1990s) due to their size nor by local networks due to their short recording period.
To analyze the data set for spatial clustering of faulting mechanisms we proceeded as follows: As a first step we defined a northward dipping layer of ~25 km thickness representing the contact zone between upper Aegean and lower African plate. In fact this zone is supposed to be thinner. However, we have to take into consideration the location error of the globally recorded events for the hypocentral depth which is supposed to be in the order of ±10 km. Furthermore, the complex geometry of the Hellenic subduction zone requires some simplification when trying to analyse the seismic activity at the plate contact zone as a whole. We refer to all events located within this layer as interplate earthquakes in the following.
In a second step, this layer was subdivided into three segments along the Hellenic arc from West to East. The dip of each segment was adjusted following structural models of the forearc region that were derived from wide angle seismics (Bohnhoff et al., 2001; Brönner, 2003), surface wave and receiver function analysis (Li et al., 2003; Meier et al., 2004a; Endrun et al., 2004) and moving source profiles (Truffert et al., 1993). Furthermore, we implement data from a Moho map of the Eastern Mediterranean (Marone et al., 2003). We defined all events above the contact zone as brittle failure within the upper Aegean plate and all events below as earthquakes within the dipping African lithosphere.
In a third step we scanned all events within the Aegean plate for spatial clustering of P and T axes. We identified four distinct subvolumes with significantly varying clustering of fault mechanisms. This resulted in a total of eight subvolumes (1-4 within the Aegean plate, 5-7 interplate seismicity, 8 within the dipping African lithosphere) that are described in the following.

3. Results:

3.1 Fault mechanisms within the Aegean plate:
Most of the fault mechanisms within the Aegean plate group into four subvolumes with significantly different types of characteristic faulting and level of clustering. Figure 5 combines these four subvolumes in a map view of their fault plane solutions and distributions of P and T axes within each subvolume. The westernmost region combines 28 events on and offshore western Crete at a maximum hypocentral depth of 17 km (subvolume 1). The events cover a magnitude range between 0.0 and 4.5. The majority of T axes trends EW at shallow plunge whereas the P axes have a dominant steep plunge and some being shallow with an average NS trend. This reflects a normal faulting regime for western Crete that is currently in the state of EW extension. In contrast, no preferred orientation of the P and T axes was identified in central Crete (subvolume 2). A total of 43 events are contained in this subvolume

most of which occurred below the Messara plain in southern central Crete down to 20 km depth. Magnitudes do not exceed M=4.4. Whereas most P axes exhibit dominant trends at N20°-70°E and N240°-280°E at varying plunge, the T axes do not exhibit any preferred orientation at all. Forming subsets based on hypocentral distribution following the main tectonic features of the Messara plain does not result in a more uniform distribution of P and T axes. The distribution of P and T axes can thus not be the result of a locally varying deformation regime, at least not at the scale resolved by the detection threshold of the local networks operated in this region. One possible explanation for such a heterogeneous distribution could be a non-uniform stress field within this subvolume. We refer to this point later in the text.
Further to the East a total of 28 events were investigated that all occurred at depth levels between 10 and 25 km below Eastern Crete (subvolume 3). The depth distribution is different to Western and Central Crete where most events occur at shallower depth. The distribution of P and T axes indicates a predominant strike-slip mechanism with components of mainly reverse but also normal faulting. Interestingly, the P axes tend to the N as well as to the S at a plunge of 20-45°. In contrast, the T axes are concentrated to N270°-320°E with a similar plunge. Thus, the fault planes are left lateral, SW/NE oriented and steeply dipping to the SE or right lateral, NW/SE oriented and steeply dipping the NE.
The easternmost subvolume 4 covers the area around the island of Karpathos and contains 13 events. These occurred at depths between 5 and 20 km and are –on average- of greater magnitude compared to the three subvolumes to the West. Although they are distributed over a much wider area than the subsets on Crete, their faulting mechanisms show a stronger clustering of P and T axes indicating an ~EW-extensional deformation within the Aegean plate between Crete and Rhodos. Comparing the four subvolumes within the upper crust with respect to their magnitude contents suggests that stronger shallow events occur more frequently in the east than in the west. This correlates with the observation that the eastern part of the Hellenic subduction zone has higher seismic activity in general (see e.g. ISC catalogue by Engdahl et al., 1998). Shallow seismic events are leaking in the Karpathos region as no local network was operated there.

3.2 Fault mechanisms of interplate seismicity:
A total of 30 events were classified as interplate earthquakes as they occurred within the three northward dipping layers of ~25km thickness as described above. In Figure 6 the three subvolumes are plotted in a map view as well as in a depth section where upper and lower boundaries of the contact zone are indicated. The three subvolumes contain 15, seven and eight events for the western, central and eastern part, respectively, and cover a magnitude range from 4.0-6.5 (smaller magnitudes were excluded as they may have larger location errors due to insufficient station coverage for regional networks on Greek territory). The P and T axes of interplate events in all three subvolumes have a preferred orientation of their deformation axes indicating shallowly N-NNE dipping thrust faulting. From the overall tectonic setting we can conclude that the steep plane does not represent the fault plane. Thus, the interplate events indicate a N-NNE trending direction of relative plate motion between the Aegean and African plates. This direction corresponds with measurements of the recent surface deformation in the south Aegean region (McClusky et al., 2000; see also black arrows in Figure 1). From west (subvolume 5) to east (subvolume 7) we observe a decreasing level of clustering of P and T axes in combination with small number of events contained in the subvolumes.
Furthermore, two of the subvolumes (5 and 7) contain a smaller number of strike-slip events that are among the best-constrained ones. The latest of these occurred in March 2004 south of Western Crete near the island of Gavdos (see Figure 6). Such events might reflect brittle failure along pre-existing faults within the upper crust although their hypocentral depth was uniformly set to 33 km as standard depth in the global catalogues. However, the overall set of interplate events indicates a N-NNE trending direction of relative motion between the Aegean and African plates that is uniform along the Hellenic arc.

3.3 Fault mechanisms of seismicity within the African lithosphere:
All hypocenters below the contact zone were identified as seismicity within the subducting African lithosphere (subvolume 8, 28 events). In Figure 7 the fault plane solutions of these events are plotted in a map view and as NS-depth section, respectively. The distribution of P and T axes differs from all other subvolumes. Whereas the compressional axes cover a wide azimuthally range (N110-270°E) at shallow plunge, the tensional axes cluster at azimuths between N300°E and N30°E at an average plunge of 45°. Thus, a relevant part of the fault mechanisms within the subducting lithosphere is similar to those

observed for the interplate seismicity (shallow thrust faulting; see Figure 6) whereas the majority of fault mechanisms have T axes parallel to the dipping direction of the slab and shallow P axes with considerable scatter of their azimuth. We interpret this distribution to reflect two different types of faulting: A group of about five events reflects a nearly identical deformation mechanism as the interplate seismicity. We classify these events as interplate events which did not match the (simplified) geometry of the contact zone assumed here due to 1. Their error in hypocenter location and 2. Local uncertainties in the existing structural models of the south Aegean region (that do not contain all local structural variations along the strike of the Hellenic arc). Thus, it is a difficult task to relate every single event to a certain type of seismicity (interplate versus in slab). Eliminating these five interplate events result in a sharper image of slab-related faulting mechanisms. The majority of events within the African lithosphere reflect slab-pull as dominant deformation mechanisms with both P and T axes being in plane with the dipping slab. The T axes point towards the dipping direction (N-NNE) whereas the P axes are dominantly trending EW.

4. Stress tensor inversion

A stress tensor inversion using the technique of Michael (1984, 1987) was applied to the catalogue as a whole as well as individually to the eight subvolumes. The algorithm uses the statistical method of bootstrap resampling and allows determining the orientation of the three principal stresses (σ_1= maximum, σ_2= intermediate and σ_3=minimum) as well as a relative stress magnitude $R=(\sigma_1- \sigma_2)/(\sigma_1- \sigma_3)$, $0<R<1$. These parameters are determined by finding the best fitting stress tensor to the observed focal mechanisms. Assumptions that need to be fulfilled by the input data are: (1) stress is uniform in the area of investigation during the observed time interval, (2) the earthquakes are shear-dislocations on pre-existing faults, and (3) slip occurs in the direction of the resolved shear stress on the fault plane.
The reliability of the deduced stress field orientation (given as the so-called misfit) reflects the level of stress field heterogeneity. We do not discuss the stress tensor inversion techniques here in detail but refer to the relevant articles where the methods themselves and their applications are entirely discussed (e.g. Gephart and Forsyth, 1984; Gephart, 1990; Michael, 1987; Michael, 1991; Hardebeck and Hauksson, 2001; Bohnhoff et al., 2004).
The inversion result for the entire catalogue reveals a well-constrained NS orientation for the maximum principal stress (σ_1) at shallow dipping angle. In contrast, no clear separation between the intermediate (σ_2) and smallest (σ_3) principal stresses could be identified when considering the 95% (2σ) confidence intervals (Figure 8). This, however, is not surprising considering the varying deformation regimes within the eight subvolumes as discussed in the previous section that are all compatible with ~NS trending shallow orientation of σ_1 but indicating different directions for σ_2 and σ_3.
Inversion results for the individual subvolumes reveal the following principal results (see Figure 9 for polar projection of the principal stress axes within each subset and Table 2 for exact values of trend and plunge of $\sigma_{1\text{-}3}$, misfit and R). Western Crete has a well-defined horizontal EW-trending direction of σ_3 whereas σ_1 and σ_2 overlap in their confidence intervals. For Central Crete no preferred orientation of the stress tensor was found which was expected due to the highly heterogeneous deformation axes contained in this subvolume. Eastern Crete reveals a well-defined orientation for σ_3 that trends EW (which is similar to Western Crete) but at 50° dipping angle. This is compatible with a left-lateral strike-slip regime with components of reverse faulting. σ_1 and σ_2 are not clearly separated in their 95% confidence intervals. However, their 68% confidence intervals do not overlap indicating a N30°E trending subhorizontal orientation for σ_1. The stress field around Karpathos is very similar to that on Western Crete but rotated clockwise by ~20°.
Inversion results for interplate seismicity should be interpreted carefully due to the comparatively small number of fault mechanisms contained in the subvolumes 5-7 (15, eight and seven events, see discussion in Bohnhoff et al., 2004). The best solutions for $\sigma_{1\text{-}3}$ are not as well constraint as for the subvolumes 1-4 discussed above. We therefore combined all fault mechanisms contained in the subvolumes 5-7 (i.e. all interplate events) to one subset. The inversion result gives clear indication for a uniform stress field along the entire part of the Hellenic arc observed here indicating a thrust faulting regime with a subhorizontal and N-NNE trending direction of σ_1. σ_3 dips at ~70° with a trend of about N50°E and σ_2 is almost horizontal trending EW.
The stress field within the African lithosphere exhibits a well defined direction for σ_3 that is trending NS at ~50° plunge. Different than for the interplate seismicity, σ_1 and σ_2 are not clearly separated but isolated at 68% confidence intervals which is well explained by the five interplate events contained in

this subvolume as discussed above. The stress field is compatible with slab pull as dominant force within the dipping slab.

5. Discussion

Western Crete reflects a clear normal faulting regime with dominant extension towards EW. Similar results were found earlier for this region based on fault plane data (Lyon-Caen, 1988; Hatzfeld et al., 1993a and 1993b; Jost et al., 2002; their data are contained in the here compiled catalogue) and from major fault trends, aerial photographs and outcropping faults (Angelier et al., 1982). Doutsos and Kokkalas (2001) identified normal faulting on Western Crete but with no preferred orientation for σ_3. Their data, however, cover also earlier stress regimes of different orientation, whereas the data base analysed in this study reflects the present (last ~50 years) tectonic setting. We interpret the present regime on Western Crete to reflect arc-parallel extension. The Karpathos area reflects a similar regime but rotated clockwise by ~20°. The orientation of the smallest principal stress is thus significantly oblique with respect to the strike of the Hellenic arc at this part (see Figure 1). This is incompatible with the interpretation given by Benetatos et al. (2004) who analysed focal mechanisms of the Aegean region. They found EW-extension for the eastern Hellenic arc and interpret this as along-arc extension (their Figures 5+6).
Obviously, the extensional domains on Western Crete and around Karpathos are decoupled from the sinistral transtensional fault zone that is located south of Central and Eastern Crete. This fault zone consists of three branches misleadingly called Ptolemeus, Pliny and Strabo 'trenches' (indicated by dotted arrows in Figure 10). The term 'trench' is misleading as these structures do not represent subduction trenches as observed at various forearcs of subduction zones worldwide but, in contrast were identified as deep-sea depressions with wedge-shaped sedimentary basins of up to 4 km thickness (Bohnhoff et al., 2001). Furthermore, these branches have a dominant sinistral strike-slip faulting (LePichon and Angelier, 1979; Huchon et al., 1982; Huguen et al., 2001). Fault mechanisms for Eastern Crete reflect a subhorizontal NE trending direction for σ_1 and a 40-50° dipping EW-trending direction for σ_3. This correlates with the main fault trend of the three deep-sea depressions which is NE to ENE (Angelier et al., 1982). Surprisingly, the fault mechanisms indicate sinistral transpression rather than transtension. The Eastern part of Crete might thus reflect a continuation of the Ptolemeus branch at slightly modified trend (ENE versus NE). This and the fact that Eastern Crete underwent significantly less stretching compared to the crust below the Libyan Sea (see Bohnhoff et al., 2001) might be responsible for the change from transtension to transpression. Furthermore this might be related to the laterally varying vertical deformation on Crete that is higher on Western and Eastern Crete compared to the central part of the island (Lambeck, 1995; their figure 14). This might also be a possible explanation of the heterogeneous stress field in Central Crete as observed here and for the high scatter of fault trends along this part of Hellenic arc in general (Angelier et al., 1982). Note, that this is different to western Crete where incipient collision is responsible for a blocked state which is probably one reason for the rapid uplift of this part of the island. The uplift seems to occur along steep normal faults as suggested by a number events contained in subvolume 1 (see Figure 5). Ten Veen and Kleinspehn (2003) report on N70°E sinistral faults on southern central Crete to play a major role within the tectonic reorganisation of the Hellenic subduction zone at about 3.4 Ma. These faults are also included in our data and could be interpreted as presently reactivated remnants of the Plio-Pleistocene deformation.

Fault mechanisms of interplate seismicity indicate a uniform N-NNE trending direction of relative plate motion between the Aegean and African plates along the Hellenic arc between the Ionian Sea and Rhodes. This confirms earlier results that partly focussed on smaller portions of the Hellenic subduction zone. McKenzie (1978) proposed N31°E and LePichon and Angelier (1979) argued for N45°E as main trend for the relative motion between Africa and Crete. Taymaz et al. (1990) analysed events at ~40 km depth and found slip vectors trending N25°E. Our data base covers the entire Hellenic arc between the Ionian Sea and Rhodes and shows that N12°E is the representative orientation of relative plate motion for this part of the Hellenic subduction zone with an accuracy of ±15° (see Figures 6 and 9). This result correlates with the GPS horizontal velocities in a Eurasia fixed reference frame (McClusky et al., 2000; see Figure 1) within the accuracy resolved here. The amphitheatrically shape of the Benioff zone as derived from the spatial distribution of hypocenters (e.g. Knapmeyer, 1999), however, is not easily explained by a uniform direction of convergence. We interpret the shape of the Benioff zone to reflect the mechanical response of the subducting plate to the curved geometry of the plate boundary. Slab pull

results in rollback and forces Crete to become the leading edge of the plate boundary. This rollback and the curved earth's surface force the plate boundary to become concave with the consequence that the slab cannot descend in a simple planar shape.
A second major consequence of the uniform direction of relative plate motion along the Hellenic arc is the significantly varying angle of its trend to the strike of the plate boundary along the arc (see Figure 10). Both directions are approximately orthogonal in the western Hellenic arc. There, an incipient collision is likely to occur at present as was also proposed by Mascle et al. (1999) and TenVeen and Kleinspehn (2003). This might also be one principal reason for the rapid uplift of this part of the island. At Central Crete both directions form an angle of 60-70° indicating a state of oblique subduction. The obliqueness increases further to the East towards Karpathos/Rhodos where it reaches a deviating angle of 40-50°.

At the central and eastern forearc, indications for remnants of oceanic lithosphere were identified by wide aperture seismic profiles (Bohnhoff et al., 2001; Brönner, 2003) that do not exceed 50 km in NS-direction as observed from surface wave studies (Meier et al., 2004a). A combined interpretation of the deformation and stress regimes within the upper plate and at the contact zone incorporating structural information suggests that the south-easternmost part of the Aegean plate advances towards the SE. This is also indicated by the GPS horizontal velocities in this region that show a small but systematically varying trend and increasing magnitudes while proceeding from west to east (Figure 11). We explain this velocity field to be initiated by the overall compressional regime due to the convergence between Aegean-Anatolia and Africa in combination with remnants of oceanic lithosphere below the eastern Libyan Sea. These remnants form the required space for plate boundary retreat and result in a counter clockwise rotation of the Eastern Hellenic arc towards the SE (see Figure 11) as indicated by the surface-velocity field and by the present deformation at depth. This regime also explains the development of the sinistral transtensional regime consisting of the Ptolemeus, Pliny and Strabo deep-sea depressions SE of Crete. Furthermore, our model requires an ESE-trending normal faulting regime between Crete and Rhodes perpendicular to the direction of present velocity field at the surface which is exactly what we observe around Karpathos. This ESE-trending extension is thus not along-arc but in direction of the retreat of the plate boundary.
Doutsos and Kokkalas (2001) argue that the transtensional regime in the eastern forearc has been established since Late Miocene then comprising NNE- to NNW-tension associated to arc-normal pull of the Aegean plate. In a second state this system then changed to ENE- and N-trending strike slip faulting as well as to NNE-trending oblique-normal faulting representing the result of strain partitioning during oblique convergence. Thus, the setup of the counter clockwise rotation of the eastern Hellenic arc might correlate with the commencing collision in the western Hellenic arc at 3.4 Ma and even expanded towards SE Turkey in the following (TenVeen, 2004).

Inversion of fault mechanisms for earthquakes within the dipping African lithosphere reveals a down-dip orientation for σ_3 at a plunge of 48° trending to the North. σ_1 was found to be oriented dominantly orthogonal to the strike of the plate boundary and vary with strike of the Hellenic arc at a plunge of 39°. This indicates that slab pull is the dominant force within the dipping African lithosphere causing gravitational instability at the southern edge of the Aegean domain and resulting in rollback of the slab especially in the East (see also LePichon and Angelier, 1979; Jackson and McKenzie, 1988). Hatzfeld et al. (1993b, based on data from a regional network) and Taymaz et al. (1990, from teleseismic recordings) observed a similar deformation regime within the slab dipping below the South Aegean. Meijer and Wortel (1996) performed forward modeling to derive the stress field in the Aegean region. They conclude that the westward Anatolian push contributes to the stress field while the existence of tension appears to be due to subduction-related forces. Both observations are in agreement with our results. Analysis of stress fields in subduction zones worldwide and its tectonic implications was pioneered by Isacks and Molnar (1971). Since then a number of paper focused on subduction-related stress fields. McGinty et al. (2000) studied the Hikurangi subduction zone (New Zealand) by inversion of focal mechanisms and identified the least compressive stress to be closely aligned with the dip of the subducting plate. Similar results were obtained for the Copiapo (northern Chile) part of the Andean subduction zone (Comte et al., 2002) and for the Alaska subduction zone by Lu et al. (1997) who also found σ_1 to be parallel along strike of the plate boundary. Christova et al. (2004) observed a down dip direction for σ_3 in the Vanuatu (New Hebrides) Wadati-Benioff zone but limited to the upper 60 km. With two exceptions our set of in-slab fault plane solutions covers the upper 100 km. As a consequence

we can not argue on the stress regime at greater depth levels but find that the stress field in the subducting lithosphere of the Hellenic subduction zone as observed for the upper 100 km is compatible with other subduction zones. However, this might be not the case for all subduction zones worldwide.

For the upper plate of the Alaska subduction zone, Lu et al. (1997) observe a non-uniform stress field reflecting strike-slip and thrusting regimes. They observe a direct relation between the size of earthquakes inverted (M>3) and homogeneity of the stress field determined. This phenomenon was also observed for fluid-injection induced seismicity at lower (-2<M<1) magnitude range (Bohnhoff et al., 2004). However, the data base of fault mechanisms from the Hellenic subduction zone give no indication for a similar relation which might be due to the smaller number of intermediate-sized (M~3) events which is explained by low seismic activity compared to other subduction zones. To perform such an investigation a long-term monitoring for the entire forearc at low threshold is required.

Conclusions

We compiled a data base of focal mechanisms for the Hellenic subduction zone in the vicinity of Crete consisting of 264 fault plane solutions that cover a magnitude range between 0 and 6.5.
Eight regions (subvolumes) were identified based on 1. Faulting regimes (upper plate, interplate, in-slab) and 2. Spatial clustering of deformation axes. Where as EW-extensional normal faulting on Western Crete was interpreted as along-arc extension, the N110°E striking direction of σ_3 in the eastern Hellenic arc reflects the SE-directed retreat of the plate boundary at this part resulting in sinistral deformation of the outer forearc. This regime extends to onshore Eastern Crete. Interplate seismicity indicates a uniform N-NNE trending direction of relative plate motion along the Hellenic arc between the Ionian Sea and Rhodes. This corresponds with the GPS-derived horizontal velocity field for this region. Rollback of the subduction zone induced by slab pull as driving mechanism forces the Benioff towards an amphitheatrically shape as observed form the distribution of hypocenters.

Acknowledgements

We acknowledge the comments by two anonymous reviewers that helped to improve an earlier version of the manuscript and discussion with J. Jackson. A. Kiratzi is thanked for helpful comments and making available her manuscript prior to publication. Furthermore, we acknowledge the focal-mechanism catalogue for eastern Crete as courtesy of J. Makris and D. Becker and contributions by O. Knabenbauer and M. Messar. We are grateful to the Deutsche Forschungsgemeinschaft (DFG) for partly funding within the Collaborative Research Centre 526 ‘Rheology of the Earth’.

References

Angelier, J., Lyberis, N., LePichon, X. and Barrier, E., 1982, The tectonic development of the Hellenic arc and the sea of Crete: A synthesis, *Tectonophysics,* **86**, 159-196.

Bath, M., 1983, The seismology of Greece, *Tectonophysics,* **98**, 165-208.

Becker, D., 2000, Mikroseismizität und Deformation der Kruste Ostkretas, Germany, *Master thesis*, Faculty of Geosciences, Hamburg University (in German).

Benetatos, C., Kiratzi, A., Papazachos, C. Karakaisis, G., 2004, Focal mechanisms of shallow and intermediate depth earthquakes along the Hellenic Arc, *J. of Geodyn.*, **37**, 253-296.

Bijwaard, H. and Spakman, W., 1998, Closing the gap regional and global travel time tomography, *J. Geophys. Res.,* **103**, 30055-30078.

Bohnhoff, M., Baisch, S., Harjes, H.-P., 2004, Focal mechanisms of induced seismicity at the superdeep German Continental Deep Drilling Program (KTB) borehole and their relation to fault structure and stress field, *J. Geophys. Res.*, **109**, B02309, doi:10.1029/2003JB002528.

Bohnhoff, M., Makris, J., Papanikolaou, D. and Stavrakakis, G., 2001, Crustal investigation of the Hellenic subduction zone using wide aperture seismic data, *Tectonophysics,* **343**, 239-262.

Brönner, M., 2003, Untersuchungen des Krustenaufbaus entlang des Mediterranen Rückens abgeleitet aus geophysikalischen Messungen, *PhD thesis*, Faculty of Geosciences, Hamburg University (in German).

Christova, C., Scholz, C.H. and Kao, H., 2004, Stress field in the Vanuatu (New Hebrides) Wadati-Benioff zone inferred by inversion of earthquake focal mechanisms: evidence for systematic lateral and vertical variations of principal stresses, *J. Geodyn.*, **37**, 125-137.

Comte, D., Haessler, H., Dorbath, L., Pardo, M., Monfred, T., Lavenn, A., Pontoise, B., Hello, Y., 2002, Seismicity and stress distribution in the Copiapo, northern Chile, subduction zone using combined on- and offshore seismic observations, *Phys. Earth Planet. Sci. Int.*, **132**, 197-217.

DeChabalier, J.B., Lyon-Caen, H., Zollo, A., Deschamps, A., Bernard, P. and Hatzfeld, D., 2002, A detailed analysis of microearthquakes in western Crete from digital three-component seismograms, *Geophys. J. Int.,* **110**, 347-360.

Delibasis, N., Ziazia, M., Voulgaris, N., Papadopoulos, T., Stavrakakis, G., Papanastassiou, D. and Drakatos, G., 1999, Microseismic activity and seismotectonics of Heraklion Area (central Crete Island, Greece), *Tectonophysics,* **308**, 237-248.

Doutsos, T. and Kokkalas, S., 2001, Stress and deformation patterns in the Aegean region, *J. Struct. Geol.*, **23**, 455-472.

Endrun, B., Meier, T., Bischoff, M. and Harjes, H.-P., 2004, Lithospheric structure in the area of Crete constrained by receiver functions and dispersion analysis of Rayleigh phase velocities, *Geophys. J. Int.*, **158**, 592-608.

Engdahl, E.R., van der Hilst, R., and Buland, R., 1998, Global teleseismic earthquake relocation with improved travel times and procedures for depth determination, *Bull. Seis. Soc. Am.,* **88**, 722-743.

Gephart, J.W., 1990, Stress and the direction of slip on fault planes, *Tectonics*, **9**, 845-858.

Gephart, J.W. and D.W. Forsyth, 1984, An improved Method for Determining the Regional Stress Tensor Using Earthquake Focal Mechanism Data: Application to the San Fernando Earthquake Sequence, *J. Geophys. Res.*, **89**, 9305-9320.

Hanka, W. and Kind, R., 1994, The GEOFON Program, *Ann. Geofis.,* **37**, 1060-1065.

Hatzfeld, D., Besnard, M., Makropoulos, K. and Hatzidimitriou, P., 1993a, Microearthquake seismicity and fault-plane solutions in the southern Aegean and its geodynamic implications, *Geophys. J. Int.,* **115**, 799-818.

Hatzfeld, D. et al., 1993b, Subcrustal Microearthquake Seismicity and Fault Plane Solutions Beneath the Hellenic Arc, *J. Geophys. Res.,* **98(B6)**, 9861-9870.

Huchon, P., Lyberis, N., Angelier, J., LePichon, X and Renard, V., 1982, Tectonic of the Hellenic Trench: a synthsis of Sea-Beam and submersible observations, *Tectonophysics,* **86**, 69-211.

Huguen, C., Mascle, J., Chaumillon, E., Woodside, J.M., Benkhelil, J., Kopf, A. and Volksonkaia, A., 2001, Deformation styles of the eastern Mediterranean Ridge and surroundings from combined swath mapping and seismic reflection profiling, *Tectonophysics,* **343**, 21-47.

Isacks, B. and Molnar, P., 1971, Distribution of stresses in the descending lithosphere from a global survey of focal-mechanism solutions of mantle earthquakes, *Rev. Geophys. Space Phys.*, **9**, 1, 103-174.

Jackson, J. and McKenzie, D.P., 1988, The relationship between plate motion and seismic moment tensors, and the rates of active deformation in the Mediterranean and Middle East, *Geophys. J.,* **93**, 45-73.

Jost, M.L., O. Knabenbauer, J. Cheng and Harjes, H.-P., 2002, Fault plane solutions of microearthquakes and small events in the Hellenic arc, *Tectonophysics,* **356**, 87-114.

Kiratzi, A. and Louvari, E., 2003, Focal mechanisms of shallow earthquakes in the Aegean Sea and the surrounding lands determined by waveform modelling: a new database, *J. Geod.,* **36**, 251-274.

Knapmeyer, M., 1999, Geometry of the Aegean Benioff zone. *Ann. Geofis.,* **42**, 27-38.

Lambeck, K., 1995, Late Pleisocene and Holocene sea-level change in Greece and southwestern Turkey: a separation of eustatic, isostatic and tectonic contributions, *Geophys. J. Int.,* **122**, 1022-1044.

LePichon, X. and Angelier, J., 1979, The Hellenic arc and trench system: a key to the neotectonic evolution of the Eastern Mediterranean area, *Tectonophysics,* **60**, 1-42.

LePichon, X., Chamot-Rooke, N. and Lallemant, S., 1995, Geodetic determination of the kinematics of central Greece with respect to Europe: Implications for Eastern Mediterranean tectonics, *J. Geophys. Res.,* **100**, 12675-12690.

Li, X., Bock, G. Vafidis, A., Kind, R., Harjes, H.-P., Hanka, W., Wylegalla, K., Meijde, M.v.d. and Yuan, X., 2003, Receiver function study of the Hellenic subduction zone: imaging crustal thickness variations and the oceanic Moho of the descending African lithosphere, *Geophys. J. Int.,* **155**, 733-748.

Lu, Z., Wyss, M. and Pulpan, H., 1997, Details of stress directions in the Alaska subduction zone from fault plane solutions, *J. Geophys. Res.,* **102 (B3)**, 5385-5402.

Lyon-Caen, H. et al., 1988, The 1986 Kalamata (south Peloponnesus) earthquake: detailed study of a normal fault, evidences for east-west extension in the Hellenic arc, *J. Geophys. Res.,* **93**, 14967-15000.

Makropoulos, K.C. and Burton, P.W., 1981, A catalogue of seismicity in Greece and adjacent areas, *Geophys. J. R. astron. Soc.,* **65**, 741-762.

Marone, F., Meijde, M.v.d., Lee, S.v.d. and Giardini, D., 2003, Joint inversion of local , regional and teleseismic data for crustal thickness in the Eurasia-Africa plate boundary region, *Geophys. J. Int.,* **154**, 499-514.

Mascle, J. et al., 1999, Images may show start of European-African plate collision, *EoS Transactions,* **80 (37)**, American Geophysical Union, 421-428.

McClusky, S. et al., 2000, Global Positioning System constraints on plate kinematics and dynamics in the eastern Mediterranean and Caucasus, *J. Geophys. Res.,* **105**, 5695-5719.

McGinty, P., Reyners, M. and Robinson, R., 2000, Stress directions in the shallow part of the Hikurangi subduction zone, New Zealand, from the inversion of earthquake first motions, *Geophys. J. Int.*, **142**, 339-350.

McKenzie, D.P., 1970, Plate tectonics of the Mediterranean region, *Nature,* **226**, 239-243.

McKenzie, D.P., 1972, Active Tectonics of the Mediterranean Region, *Geophys. J. R. astr. Soc.,* **30**, 109-185.
McKenzie, D.P., 1978, Active Tectonics of the Alpine-Himalayan belt : the Aegean Sea and surrounding regions, Geophys. *J. R. astron. Soc.*, **55**, 217-254.
Meier, T., Dietrich, K., Stöckhert, B. and Harjes, H.-P., 2004a, One-dimensional models of shear wave velocity for the eastern Mediterranean obtained from the inversion of Rayleigh wave phase velocities and tectonic implications, *Geophys. J. Int.,* **156**, 45-58.
Meier, T., Rische, M., Endrun, B., Vafidis, A. and Harjes, H.-P., 2004b, Seismicity of the Hellenic subduction zone in the area of western and central Crete observed by temporary local seismic networks, *Tectonophysics*, **383**, 149-169.
Meijer, P.Th. and Wortel, M.J.R., 1996, Temporal variation in the stress field of the Aegean region, *Geophys. Res. Lett.,* **23 (5)**, 439-442.
Meulenkamp, J.E.,Wortel, M.J.R., VanWamel, W.A., Spakman and Hoogerduyn Strating, E., 1988, On the Hellenic subduction zone and the geodynamic evolution of Crete since the late Middle Miocene, *Tectonophysics*, **146**, 203-215.
Michael, A.J., 1984, Determination of stress from slip data; faults and folds, *J. Geophys. Res.*, **89**, 11517-11526.
Michael, A.J., 1987, Use of focal mechanisms to determine stress: a control study, *J. Geophys. Res.*, **92 (B1)**, 357-368.
Michael, A.J., 1991, Spatial variations in stress within the 1987 Whittier Narrows, California, aftershock sequence: New techniques and results, *J. Geophys. Res.*, **96**, 6303-6319.
Papadimitriou, E., 1993, Focal mechanisms along the convex side of the Hellenic arc. *Bollettino de Geofisica Teorica et Applicata*, **XXXV**, 401-426.
Papadopoulos, G.A., Kondopoulou, D., Leventakis, G.-A. and Pavlides, S., 1986, Seismotectonics of the Aegean region, *Tectonophysics,* **124**, 67-84.
Papazachos, B.C., 1973, Distribution of seismic foci in the Mediterranean and surrounding area and its tectonic implications, *Geophys. J.R. astron. Soc.,* **33**, 421-430.
Papazachos, B.C. and Papazachou, C.B., 1997, The earthquakes of Greece, Ziti (ed.), Technical books editions, Thessaloniki, 304pp.
Papazachos, B.C., Kiratzi, A. and Papadimitriou, E., 1991, Regional Focal Mechanisms for Earthquakes in the Aegean Area, *PAGEOPH,* **126 (4)**, 405-420.
Papazachos, B.C., Karakostas, V.G., Papazachos, C.B. and Scordilis, E.M., 2000, The geometry of the Wadati-Benioff zone and lithospheric kinematics in the Hellenic arc, *Tectonophysics,* **319**, 275-300.
Snoke, J.A., 2003, FOCMEC: FOcal MEChanism determinations, *International Handbook of Earthquake and Engineering Seismology,* W.H.K. Lee, H. Kanamori, P.C. Jennings and Kisslinger, C. (eds.), Academic Press, San Diego, Chapter 85.12.
Snoke, J.A., Munsay, J.W., Teague, A.G. and Bollinger, G.A., 1984, A program for focal mechanism determination by combined use of polarity and SV-P amplitude ratio data, *EQ Notes,* **55 (3)**, 15.
Spakman, W., Wortel, M.J.R. and Vlaar, N.J., 1988, The Hellenic subduction zone: a tomographic image and its geodynamic implication, *Geophys. Res. Lett.,* **15**, 60-63.
Taymaz, T., Jackson, J. and Westaway, R., 1990, Earthquake mechanisms in the Hellenic trench near Crete, *Geophys. J. Int.,* **102**, 695-731.
TenVeen, J.H., 2004, Extension of Hellenic forearc shear zones in SW Turkey: the Pliocene-Quartenary deformation of the Esen Cay Basin, *J. Geodyn.*, **37**, 181-204.
TenVeen, J.H. and Kleinspehn, K.L., 2003, Incipient continental collision and plate-boundary curvature: Late Pliocene-Holocene transtensional Hellenic forearc, Crete, Greece, *J. Geol. Soc. London,* **160**, 161-181.
Truffert, C., Chamot-Rouke, N., Lallemant, S., DeVoogd, B., Huchon, P. and LePichon, X., 1993, The crust of the western Mediterranean Ridge from deep seismic data and gravity modelling, *Geophys. J. Int.,* **114**, 360-372.

FIGURES AND CAPTIONS:

Figure 1:

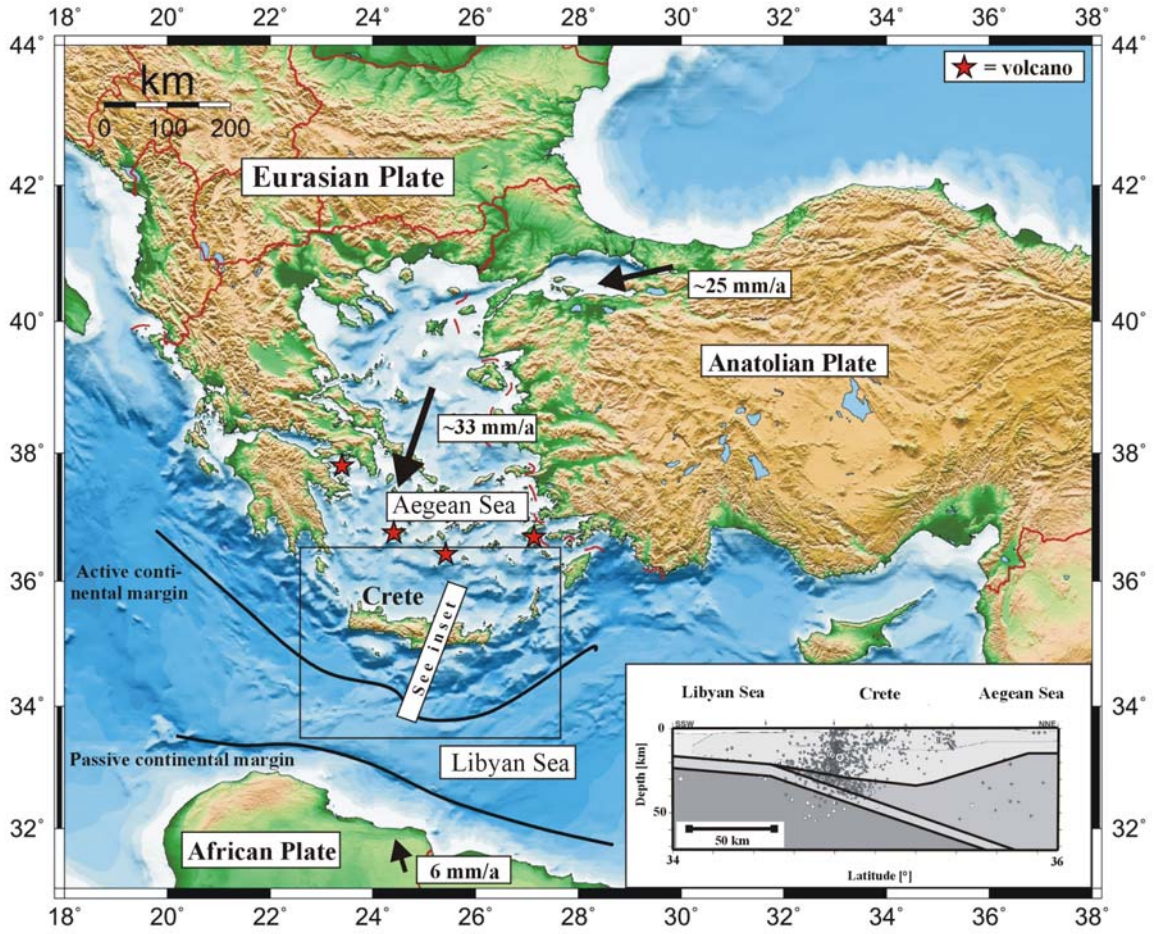

Figure 1: Location map of the Aegean-Anatolian region and its main tectonic elements. The Hellenic Arc is part of the forearc and consists of a number of islands of which Crete is the largest. Stars indicate active volcanic centers along the Hellenic volcanic arc ~150km north of the Hellenic Arc. Bold arrows indicate surface displacement rates with respect to stable Eurasia that are representative for each region (simplified after McClusky et al., 2000). The transect A-B is parallel to the dipping direction of the African lithosphere and shown as a depth section in the lower right. It combines results from microseismicity and surface wave studies in the Hellenic subduction zone (after Meier et al., 2004b). The rectangle marks the area investigated in this study.

Figure 2:

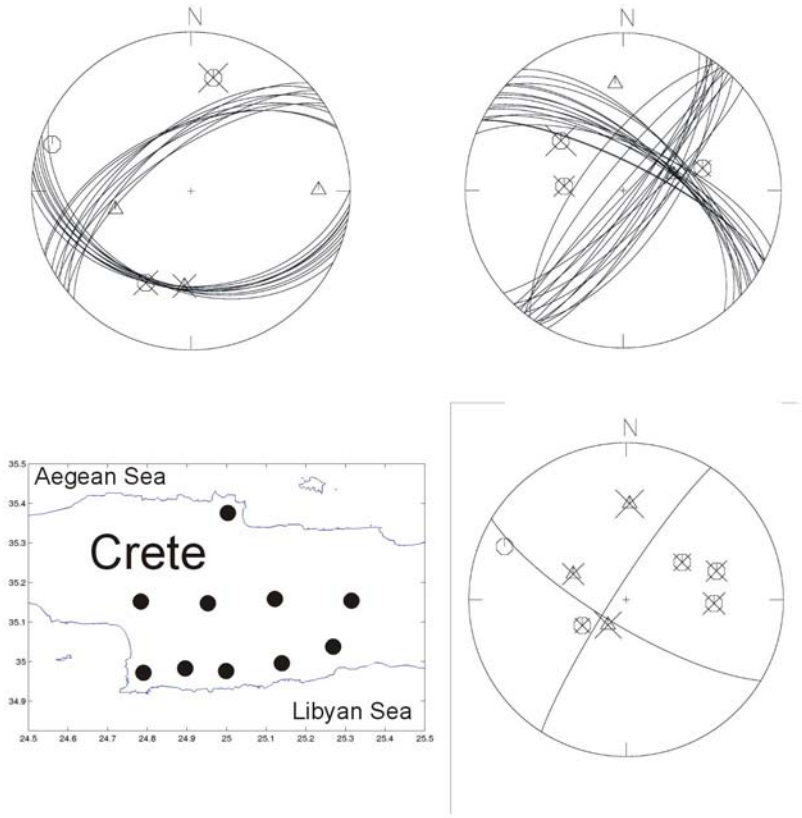

Figure 2: Selected fault plane solutions for earthquakes recorded by the temporal network on southern central Crete. Projection is lower hemisphere. Circles and diamonds represent compressional and dilatational first motions of the P wave, respectively. Crosses indicate stations for which SH/P amplitude ration were determined. In the lower left the station distribution of our seismic network and two permanent station of the GEOFON network are shown.

Figure 3:

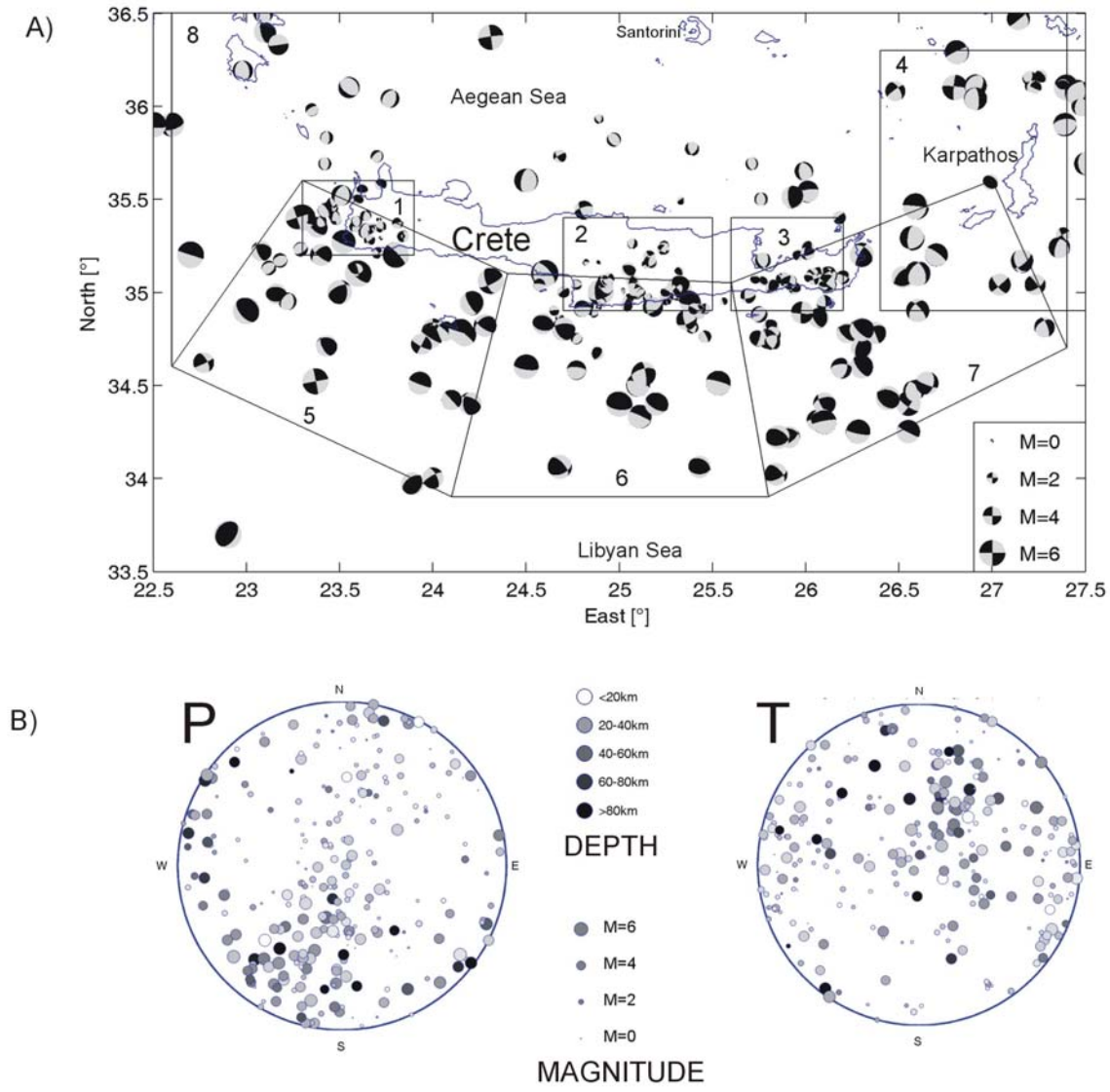

Figure 3: a) Data set analysed in this study. Shown is the lower hemisphere projection of all 264 fault plane solutions that were collected or determined, respectively (see text for details). The size of the beachballs is scaled to event magnitude. The polygons show the surface boundaries of the subvolumes 1-8 that were identified based on types of faulting (seismicity within the Aegean plate, interplate seismicity and seismicity within the dipping African lithosphere) and spatial clustering of faulting mechanisms (for seismicity within the Aegean plate): 1=Aegean plate, Western Crete; 2=Aegean plate, Central Crete; 3= Aegean plate, Eastern Crete; 4= Aegean plate, Karpathos area; 5= interplate seismicity, Western Hellenic arc; 6= interplate seismicity, Central Hellenic arc; 7=interplate seismicity, Eastern Hellenic arc; 8=seismicity within the dipping African lithosphere.
b) Distribution of P (left) and T (right) axes for all 264 fault plane solutions in equal area lower hemisphere projection. Size of circles is scaled with magnitude and shading indicates hypocentral depth.

Figure 4:

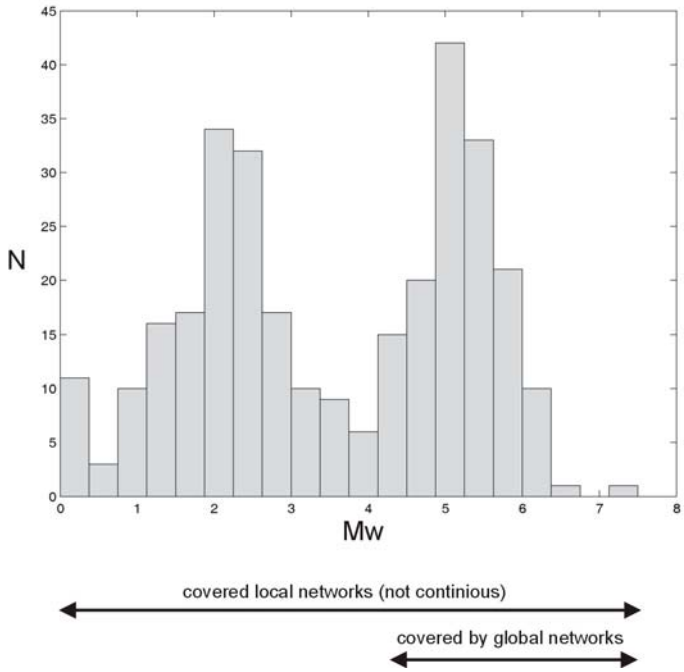

Figure 4: Magnitude frequency for the entire set of fault mechanisms investigated in this study. The catalogue covers the time interval 1959-2004 and is complete for M≥5. A large number of events with small magnitudes where recorded by local networks in distinct regions during several months. Therefore this catalogue is somewhat heterogeneous (see text).

Figure 5:

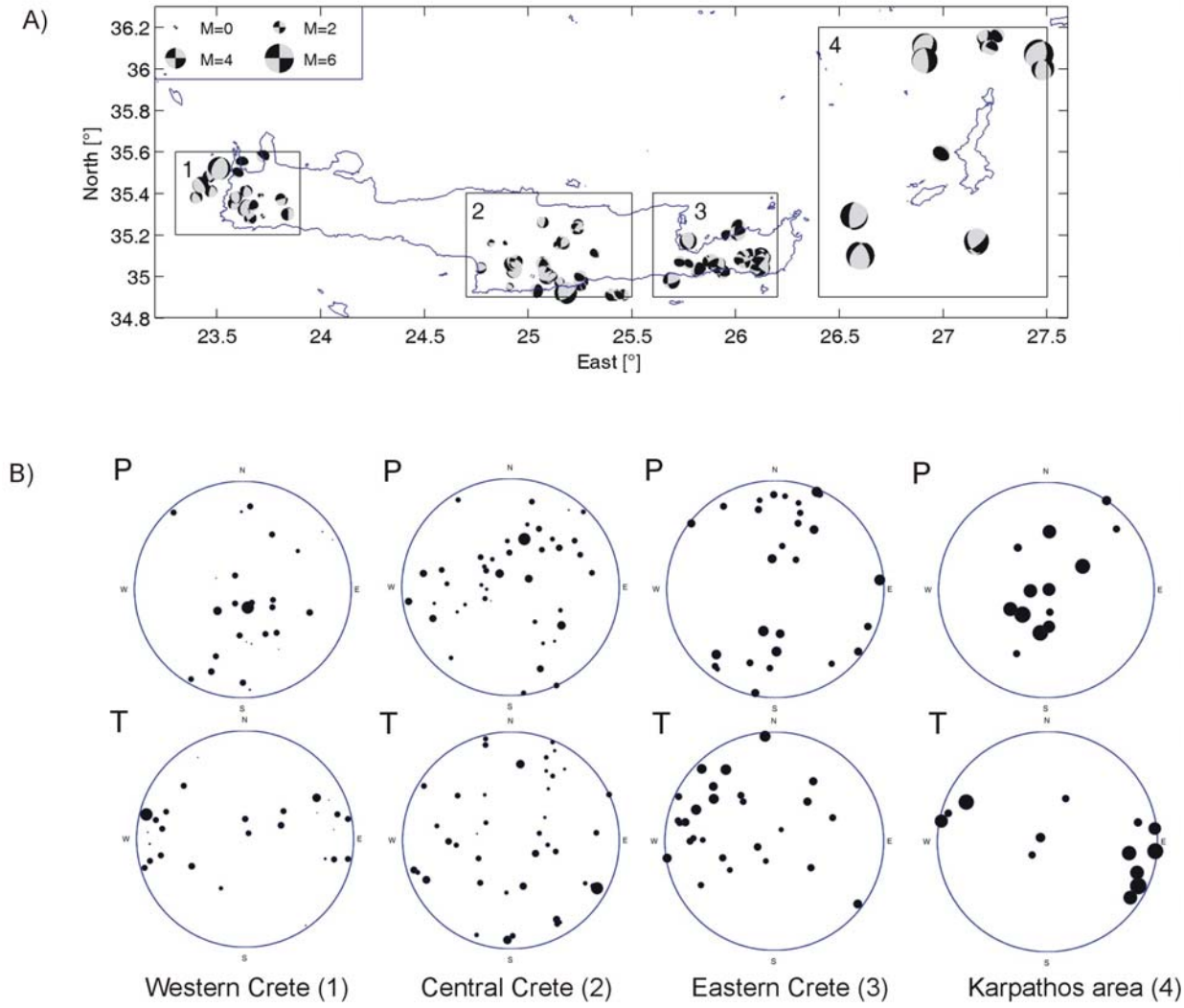

Figure 5 : a) Map view of all fault plane solutions for earthquakes within the Aegean plate that are contained in subvolumes 1-4 (see Figure 3a).
b) Distributions of P (top) and T (bottom) axes for each of the four subvolumes. Size of circles scales with magnitude and is enlarged by a factor of two compared to Figure 3b.

Figure 6 :

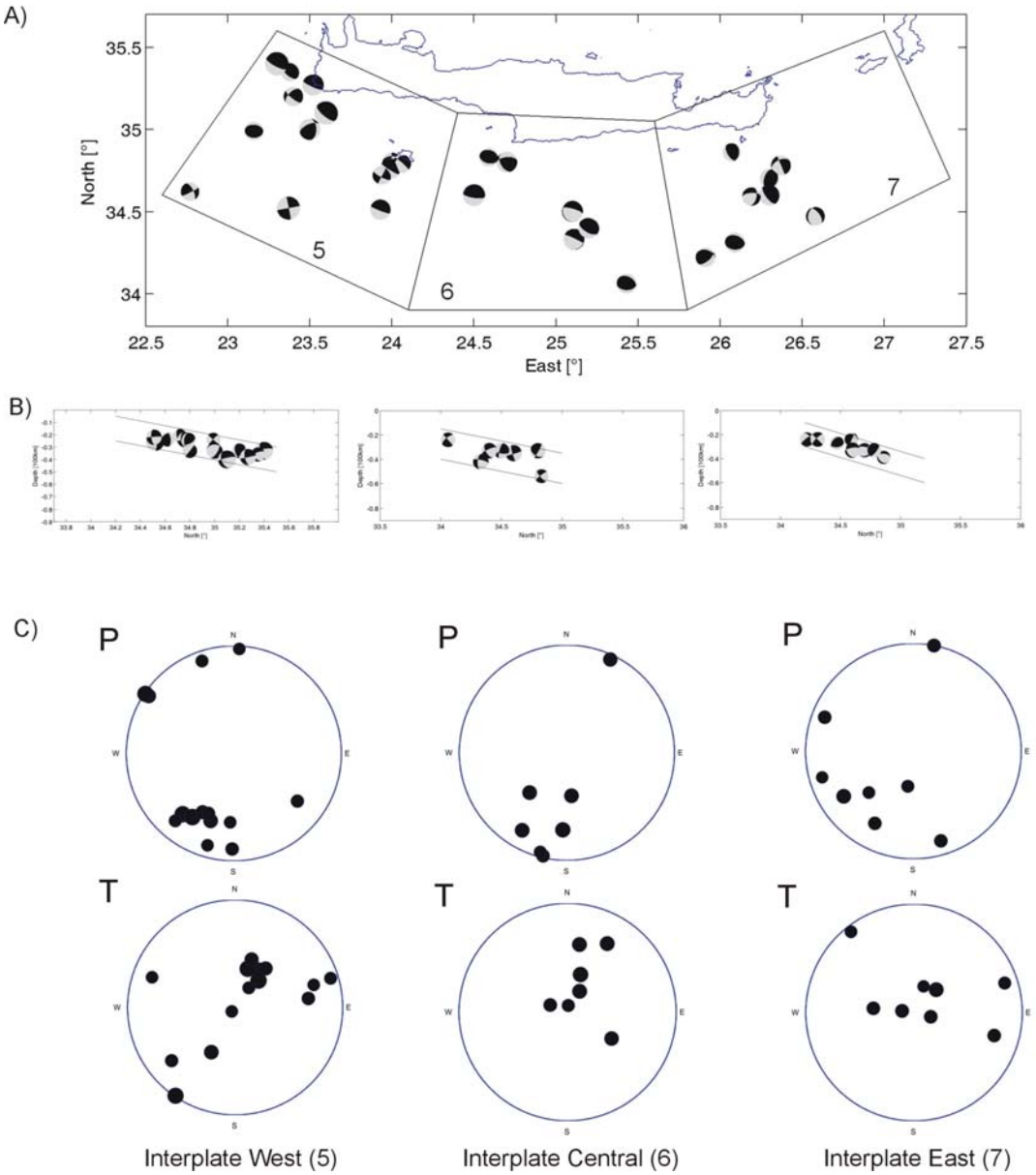

Figure 6 : a) Map view of all fault plane solutions for earthquakes within the contact zone between upper (Aegean) and lower (African) plate subdivided into three segments along the Hellenic Arc from West to East (subvolumes 5-7, see Figure 3a).
b) Depth sections for the three subvolumes shown in 6a). Upper and lower boundaries for the contact zone were fixed based on existing structural models of the Hellenic subduction zone taking into consideration the depth error for events located with global networks (~10km). Note that the beachballs are rotated according to the viewers' perspective, i.e. lower hemisphere projection, seen from the East.
c) Distributions of P (top) and T (bottom) axes for each of the three subvolumes. Size of circles scales with magnitude and is enlarged by a factor of two compared to Figure 3b.

Figure 7 :

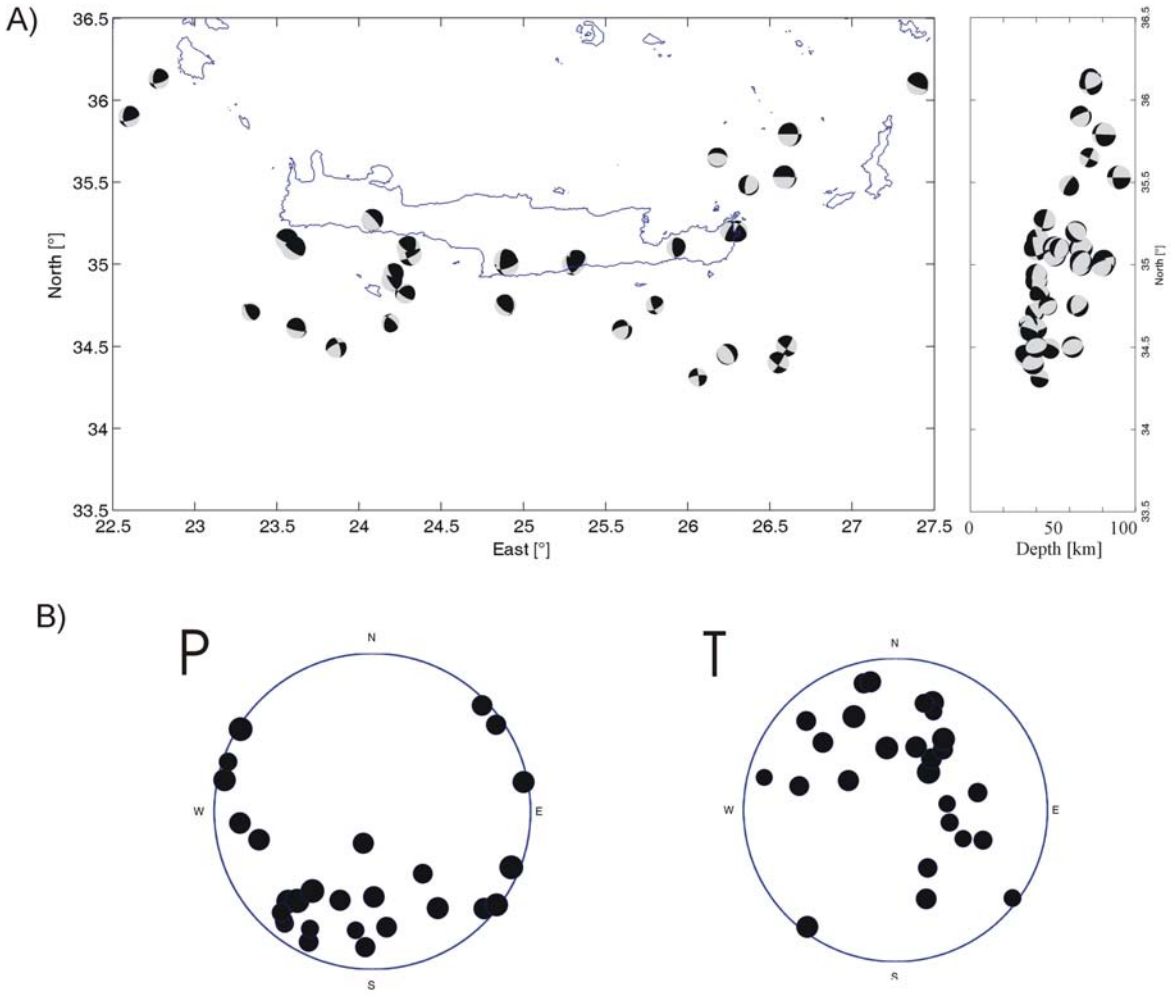

Figure 7 : a) Map view and depth section of all fault plane solutions for earthquakes within the subducting African lithosphere (subvolume 8, see Figure 3a). In the depth section the beachballs are rotated according to the viewers direction, i.e. lower hemisphere projection seen from the East.
b) Distribution of P (left) and T (right) axes within subvolume 8. Size of circles scales with magnitude and is enlarged by a factor of two compared to Figure 3b.

Figure 8 :

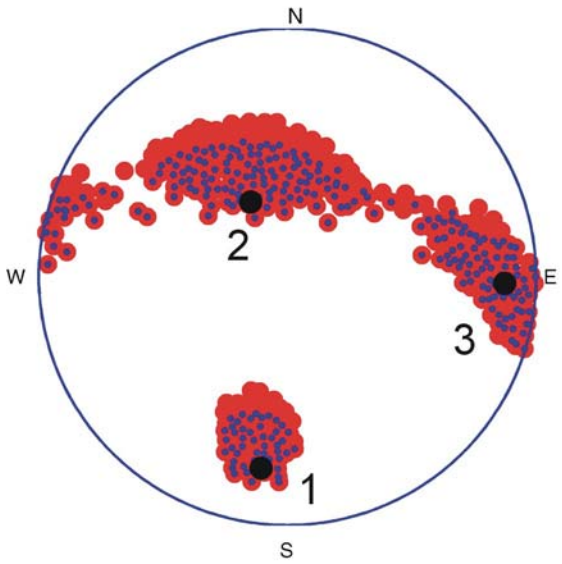

Figure 8 : Result of stress tensor inversion for the entire catalogue containing 264 fault plane solutions (see Figure 3a). Bold black dots represent the best fitting orientations for the three principal stresses (1=maximum, 2=intermediate ; 3=minimum). Small black dots and large gray dots represent the 1σ (68%) and 2σ (95%) confidence intervals.

Figure 9 :

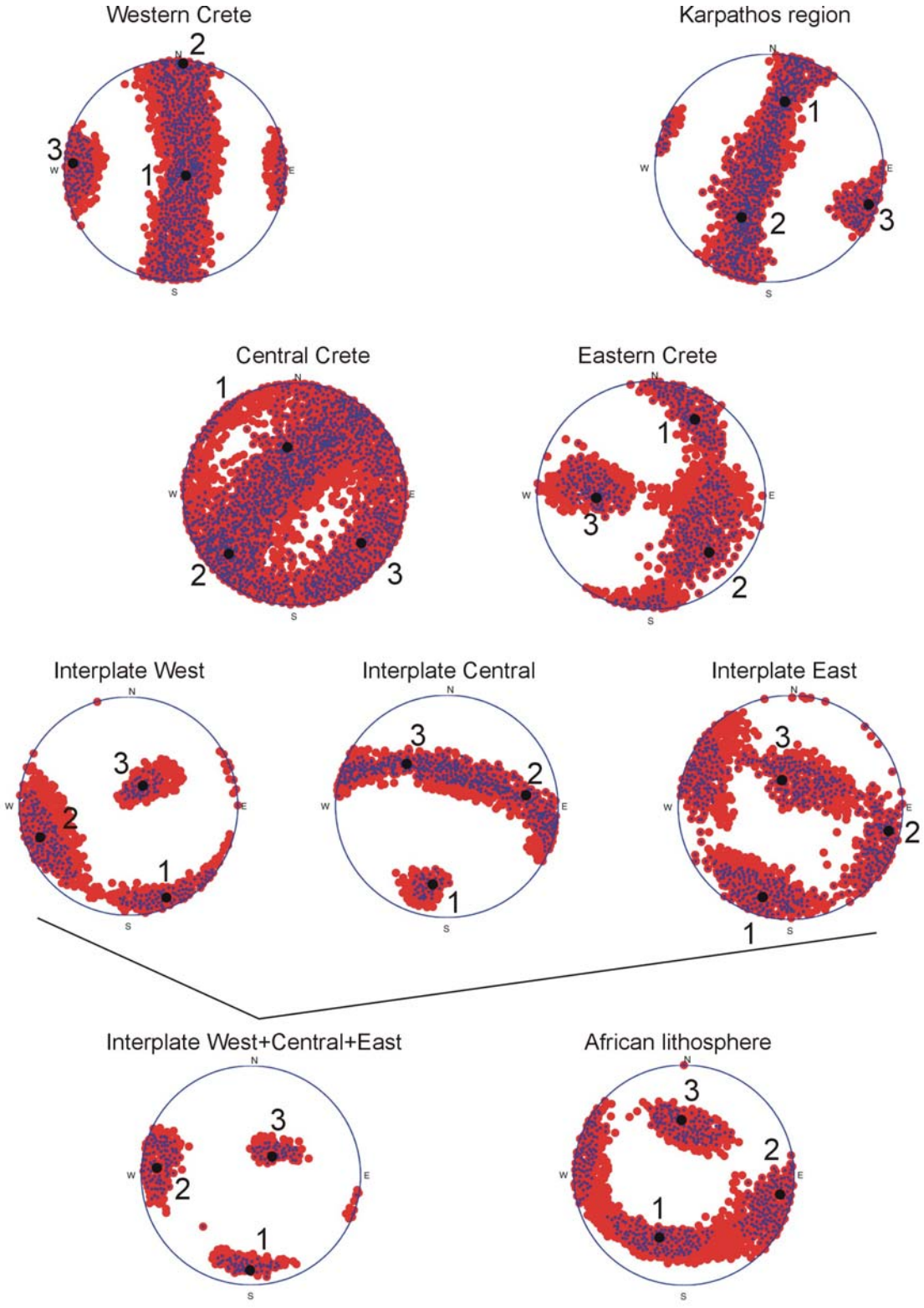

Figure 9 : Results of stress tensor inversion for the eight subvolumes and for the entire set of interplate events as combination of subvolumes 5-7. For explanation of symbols see Figure 8.

Figure 10 :

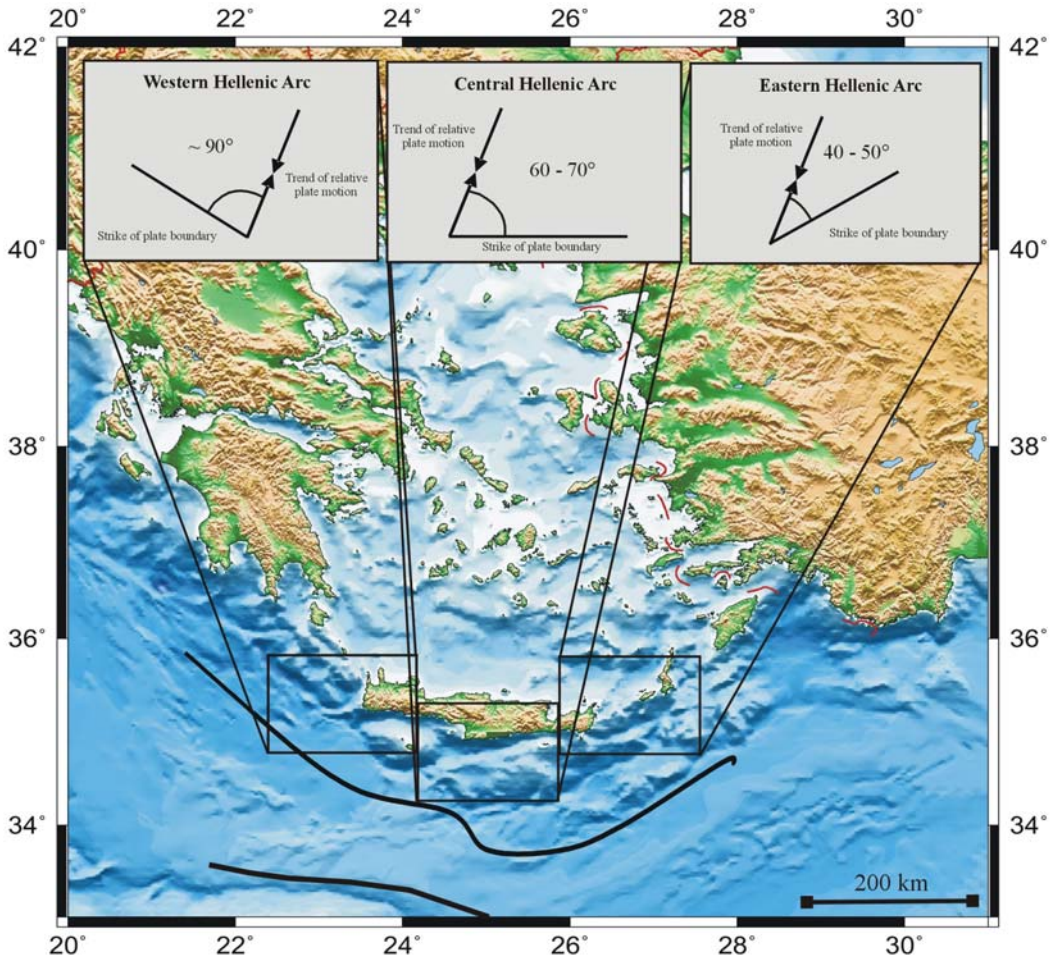

Figure 10: Angle between the direction of relative plate motion (that was identified to be uniform along the Hellenic arc) and the strike of the plate boundary for the Western, Central and Eastern Hellenic arc. Arrows indicate the deformation regime within the upper Aegean plate along the Hellenic arc as determined in this study. Dotted arrows mark the sinistral transtensional fault zone at the Ptolemeus, Pliny and Strabo deep sea depressions. Black lines indicate the active and passive continental margin, respectively.

Figure 11 :

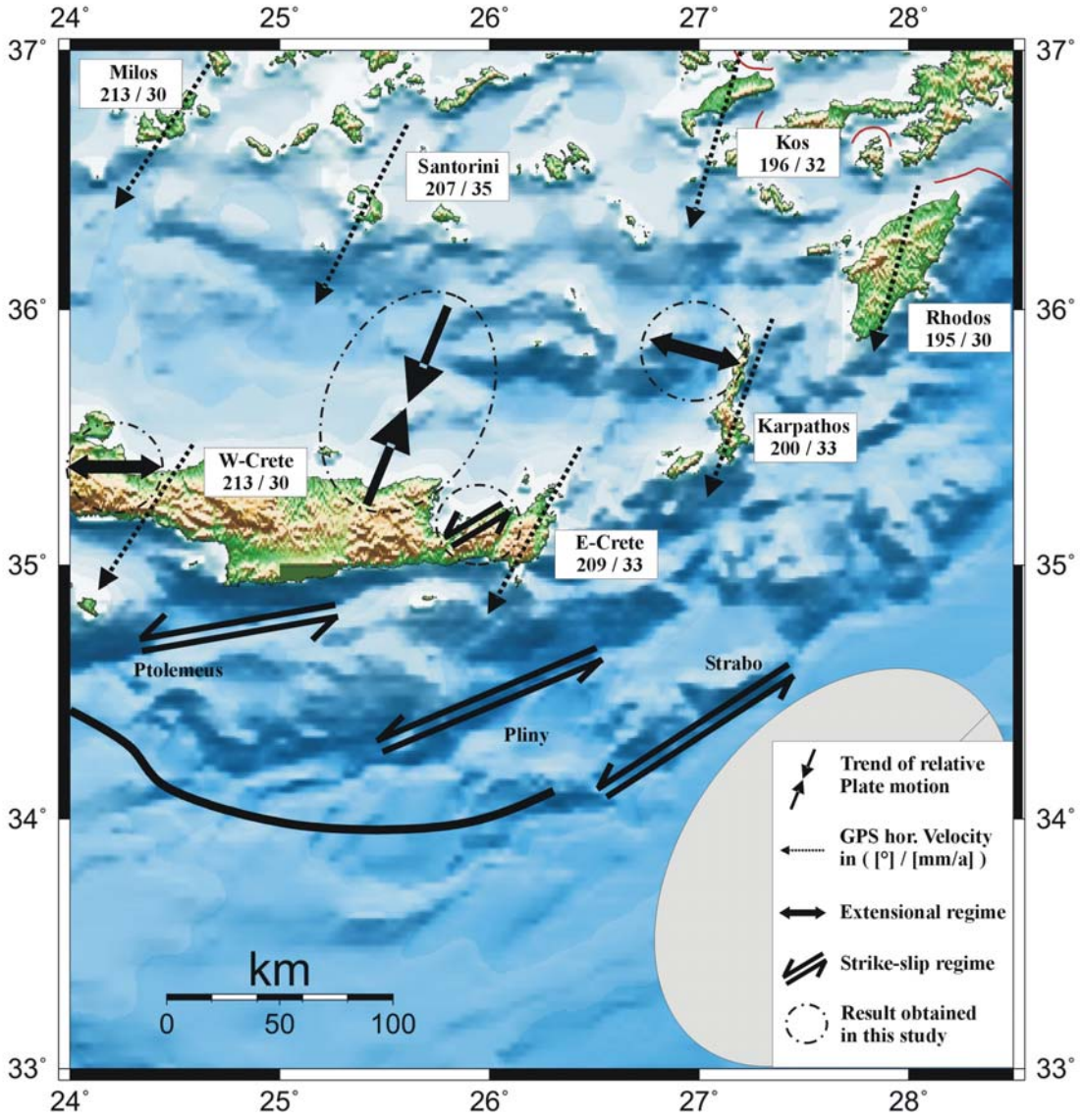

Figure 11 : Summary of results focussing on the eastern Hellenic arc. Dotted arrows indicate strike (direction) and magnitude of the GPS-derived velocity field at the surface (after McClusky et al., 2000) that shows second order variations in the south-east Aegean region. Convergent black arrows indicate the direction of relative plate motion (uniform along the Hellenic arc) and divergent black arrows indicate the trend of extension on Western Crete and in the Karpathos area. Remnants of oceanic crust southeast of the Hellenic arc (indicated by the gray ellipse) form space for retreatment of the plate boundary at this part of the Hellenic as which correlates with the counterclock wise rotation of GPS-derived trend of surface deformation while proceeding from West to East.

TABLES AND CAPTIONS:

Table 1 :

YEAR	MONTH	DAY	HOUR	MIN	LAT [°N]	LON [°E]	DEPTH [km]	MAG	STRIKE	DIP	RAKE	SOURCE
1959	05	14	06	36	35.10	24.60	43	6.3	319	67	-110	PDO
1962	01	26	08	17	35.20	22.70	33	6.2	108	90	90	PDO
1962	04	28	11	18	36.10	26.80	33	5.8	275	85	-174	PDO
1965	04	09	23	57	35.10	24.30	67	6.1	23	56	158	PPA-
1965	04	09	23	57	35.10	24.30	51	6.0	280	77	-134	PDO-
1965	04	09	23	57	35.06	24.31	51	6.0	63	76	157	TAY*
1965	04	27	14	09	35.70	23.50	50	5.5	140	59	-77	MCK-
1965	04	27	14	09	35.60	24.50	13	5.4	191	65	-79	KIR*
1965	04	27	14	09	35.60	23.50	5	5.7	22	27	-81	PPA-
1965	11	28	05	26	36.30	27.50	89	5.8	246	21	349	MCK
1965	11	28	05	26	36.10	27.40	73	6.0	350	30	142	PPA*
1966	03	11	20	01	34.40	24.20	33	5.1	296	59	47	PDO
1966	05	09	00	42	34.40	26.40	20	5.8	295	40	90	MCK(*)
1966	05	09	00	42	34.40	26.40	33	5.8	115	50	89	PDO(*)
1966	05	09	00	42	34.40	26.40	10	5.8	295	40	90	PPA(*)
1966	05	09	00	42	34.43	26.44	16	5.5	132	46	110	TAY*
1966	11	19	07	12	35.00	23.50	33	5.5	245	61	136	PDO
1968	07	08	17	41	34.50	25.10	33	5.4	286	75	-107	PDO
1968	08	15	02	29	35.20	26.70	33	5.2	306	78	-90	PDO
1968	10	19	15	34	35.20	23.40	33	4.9	128	77	147	PDO
1969	04	16	23	21	35.34	27.47	45	5.2	309	32	98	MCK(*)
1969	06	12	15	13	34.40	25.00	19	6.1	294	29	105	PPA*
1969	06	12	15	13	34.40	25.06	25	5.8	294	29	105	MCK(*)
1969	06	12	15	13	34.40	25.00	33	6.1	95	62	90	PDO(*)
1969	06	12	15	13	34.43	25.04	19	5.8	163	50	44	TAY-
1971	01	03	23	18	34.90	26.30	2	5.4	144	70	86	MCK(*)
1971	01	03	23	18	34.60	26.30	33	5.4	143	69	85	PDO*
1972	04	29	18	29	34.80	24.70	33	5.3	264	61	44	PDO
1972	05	04	21	3	35.10	23.60	40	6.2	309	18	89	KIR*
1972	05	04	21	39	35.10	23.60	33	6.5	106	86	90	PDO(*)
1972	05	04	21	39	35.10	23.60	40	6.5	308	18	90	PPA(*)
1972	05	04	21	39	35.15	23.56	41	5.9	112	74	98	TAY(*)
1973	04	06	14	13	34.40	25.20	33	5.4	120	63	90	PDO
1973	06	26	19	05	34.40	26.10	33	5.0	151	70	144	PDO
1973	10	14	18	07	34.70	26.30	33	4.9	200	58	88	PDO
1973	11	29	00	00	35.20	23.80	1	6.0	316	10	90	MCK*
1973	11	29	10	57	35.20	23.80	18	5.7	283	38	97	PDI(*)
1973	11	29	10	57	35.20	23.80	33	6.0	139	82	90	PDO(*)
1973	11	29	10	57	35.20	23.80	1	6.0	316	10	90	PPA(*)
1973	11	29	10	57	35.18	23.81	18	5.7	224	67	10	TAY-
1975	01	09	18	53	34.80	24.00	33	4.8	178	88	-38	PDO
1975	09	17	23	04	36.40	23.10	33	5.1	167	67	117	PDO
1975	09	22	00	44	35.20	26.30	64	5.5	310	50	17	PPA*
1975	09	22	00	44	35.20	26.26	64	5.4	209	75	131	TAY(*)
1977	08	18	09	27	35.27	24.08	45	5.7	85	15	-142	CMT(*)
1977	08	18	09	27	35.30	23.50	38	5.6	270	12	114	PPA(*)
1977	08	18	09	27	35.27	23.52	38	5.5	114	79	96	TAY*
1977	09	11	23	19	34.90	23.00	19	6.3	320	30	90	PPA*
1977	09	11	23	19	34.51	22.99	37	5.8	74	28	100	CMT-
1977	09	11	23	19	34.90	23.00	16	5.8	295	40	95	PDI(*)
1977	09	11	23	19	34.90	23.00	33	6.3	165	76	124	PDO(*)
1977	09	11	23	19	34.95	23.05	19	5.8	276	47	89	TAY(*)
1978	03	07	22	33	34.19	25.45	34	5.5	225	14	40	CMT(*)
1978	03	07	22	33	34.33	25.11	42	5.4	42	18	-162	BEN*
1979	05	15	06	59	34.60	24.50	35	5.7	253	17	65	PPA*
1979	05	15	06	59	34.38	24.80	15	6.1	172	4	-20	CMT(*)
1979	05	15	06	59	34.58	24.45	35	5.5	253	17	65	TAY(*)
1979	06	15	11	34	34.82	24.42	33	5.4	216	11	10	CMT(*)

1979	06	15	11	34	34.94	24.21	40	5.5	150	75	70	TAY*
1979	06	15	11	34	34.90	24.20	40	5.6	21	23	141	PPA(*)
1979	07	23	11	41	35.29	26.57	15	5.6	61	35	-40	CMT*
1979	07	23	11	41	35.50	26.40	11	5.5	61	35	-40	PPA(*)
1979	08	22	20	12	35.90	27.39	68	5.3	64	31	-106	BEN
1981	09	13	23	25	34.56	25.13	15	5.5	256	65	-11	CMT
1982	08	17	22	22	33.70	22.90	23	6.3	219	34	70	CMT(*)
1982	08	17	22	22	33.70	22.90	9	6.4	219	34	93	PPA*
1982	08	17	22	22	33.71	22.94	39	6.0	230	45	109	TAY(*)
1982	08	17	22	22	33.77	22.96	10	6.4	196	28	69	USG(*)
1983	01	03	00	12	33.97	23.89	102	5.1	30	36	70	CMT
1983	03	19	21	41	34.75	24.89	65	5.6	358	39	131	CMT-
1983	03	19	21	41	35.00	25.30	67	5.7	43	51	139	PPA(*)
1983	03	19	21	41	35.02	25.32	67	5.7	44	51	139	TAY*
1984	05	22	13	57	36.13	22.78	73	5.1	182	55	29	CMT(*)
1984	05	22	13	57	35.90	22.60	67	5.5	182	55	29	PPA*
1984	05	22	13	57	35.90	22.60	63	5.1	188	44	32	BEN(*)
1984	06	21	10	43	35.74	23.80	34	6.2	79	7	-128	CMT(*)
1984	06	21	00	00	35.40	23.30	33	6.2	322	16	114	PDI*
1984	06	21	10	43	35.40	23.30	39	6 .2	322	16	114	PPA(*)
1984	06	21	10	43	35.31	23.28	39	5.8	110	72	83	TAY(*)
1985	09	27	16	39	34.05	26.94	44	5.6	135	76	13	CMT(*)
1985	09	27	16	39	34.50	26.60	40	5.5	125	77	9	PPA(*)
1985	09	27	16	39	34.40	26.55	38	5.6	125	77	9	TAY*
1986	05	22	19	52	34.12	26.72	33	5.5	227	37	24	CMT(*)
1986	05	22	19	52	34.25	26.55	27	5.3	118	86	99	BEN*
1986	07	16	02	55	36.04	23.77	21	4.0	14	50	-108	HAT
1987	04	12	02	47	35.40	23.27	15	5.1	252	90	180	CMT
1988	07	11	15	54	35.07	25.73	8	1.8	280	60	95	HAT
1988	07	13	11	22	35.06	25.77	13	1.6	125	55	89	HAT
1988	07	15	19	25	35.02	25.31	28	1.9	319	90	18	HAT
1988	07	15	22	55	35.69	25.71	9	2.4	157	50	-107	HAT
1988	07	20	02	09	35.82	24.97	24	2.8	140	50	-90	HAT
1988	07	25	11	11	34.88	25.75	8	3.4	40	50	-90	HAT
1988	07	25	14	45	35.40	26.18	18	2.6	230	77	105	HAT
1988	07	26	21	56	36.11	27.21	14	2.6	209	54	-71	HAT
1988	07	26	23	40	36.15	27.20	15	2.8	14	70	-54	HAT
1988	07	27	05	00	35.44	24.81	29	4.1	253	70	-158	HAT
1988	07	27	10	55	35.50	25.76	24	2.6	350	50	-104	HAT
1988	07	31	21	39	36.11	27.38	23	2.5	94	55	85	HAT
1988	08	01	16	45	35.73	23.70	17	2.4	230	60	-67	HAT
1988	08	02	11	25	35.50	23.61	12	99	230	70	-40	DEC-
1988	08	02	11	25	35.50	23.60	13	1.9	120	50	90	HAT*
1988	08	03	08	09	35.73	24.68	19	2.5	240	80	25	HAT
1988	08	04	05	26	35.45	23.45	27	3.1	270	50	-61	HAT
1988	08	04	06	00	36.16	27.26	19	2.5	319	60	90	HAT
1988	08	04	11	43	35.34	23.67	1	2.0	199	59	47	HAT
1988	08	04	18	43	35.23	23.29	29	2.9	59	60	-92	HAT
1988	08	05	05	21	35.17	23.18	21	2.9	250	50	-90	HAT
1988	08	05	12	53	35.65	25.99	25	4.0	179	56	-67	HAT
1988	08	05	22	37	36.10	27.23	12	2.4	114	80	89	HAT
1988	08	06	04	21	35.31	27.38	26	2.8	60	90	170	HAT
1988	08	10	01	06	35.13	23.12	20	2.9	40	50	-110	HAT
1988	08	13	22	29	35.59	26.99	13	3.3	118	45	82	HAT
1988	08	14	02	30	35.44	23.42	4	2.9	327	70	-94	HAT
1988	08	14	13	28	35.58	23.72	11	2.2	127	68	111	HAT
1988	08	14	16	13	35.55	23.62	11	2.1	90	60	90	HAT
1988	08	15	05	37	35.35	23.58	8	1.9	199	69	-90	HAT*
1988	08	15	05	37	35.36	23.58	9	99	170	70	-75	DEC(*)
1988	08	15	20	08	35.12	25.05	20	2.8	140	50	119	HAT
1988	08	18	13	10	34.95	23.22	23	3.8	214	51	-67	HAT
1988	08	18	18	07	35.12	23.59	22	2.4	345	78	137	HAT*
1988	08	18	18	07	35.15	23.61	23	99	225	75	35	DEC-
1988	08	19	17	12	35.98	23.35	19	2.5	239	69	-90	HAT

1988	08	20	12	16	35.39	23.48	24	99	170	85	-110	DEC
1988	08	20	14	29	35.69	23.42	13	2.5	7	51	-78	HAT
1988	08	20	15	32	35.77	25.39	16	2.8	159	59	-137	HAT
1988	08	22	11	05	35.83	23.43	27	2.5	359	63	-104	HAT
1988	08	27	04	50	35.34	23.64	4	99	0	50	-105	DEC
1988	08	27	15	12	35.32	23.63	3	99	175	50	-75	DEC
1988	08	29	21	07	35.37	23.81	4	99	255	85	-45	DEC
1988	09	02	22	09	35.28	23.66	5	99	145	60	-175	DEC
1988	09	03	15	29	35.38	23.59	3	99	360	50	-75	DEC
1988	09	05	20	03	34.51	26.65	15	5.2	15	55	-11	CMT
1988	09	07	03	22	35.41	23.64	5	99	195	65	-50	DEC
1988	09	12	07	36	35.49	23.48	12	99	195	70	-80	DEC
1988	09	12	14	56	35.41	23.47	8	99	195	75	-55	DEC
1988	09	12	22	18	35.21	23.70	29	99	60	75	-165	DEC
1988	09	13	08	06	35.38	23.40	8	99	320	65	-125	DEC
1988	09	13	10	01	35.48	23.46	10	99	160	75	-135	DEC
1988	09	16	03	42	35.35	23.72	76	99	110	70	-150	DEC
1989	03	17	05	42	34.51	25.53	17	5.7	77	10	-118	CMT
1989	03	28	13	29	34.06	24.68	56	5.5	67	53	29	CMT
1989	06	14	18	06	34.30	26.10	15	5.5	102	8	-68	CMT
1989	08	27	01	21	34.25	26.28	15	5.6	223	19	33	CMT
1990	07	09	11	22	34.45	26.24	33	5.4	129	27	-106	CMT-
1990	07	09	11	22	34.90	26.60	9	5.2	217	56	-21	KIR*
1990	07	09	11	22	34.90	26.60	19	5.5	327	64	-82	PPA-
1991	03	19	12	09	34.60	26.13	15	5.5	245	36	-33	CMT-
1991	03	19	12	09	34.80	26.30	12	5.5	261	30	40	KIR*
1991	03	19	12	09	34.80	26.30	7	5.8	2	71	-122	PPA
1992	04	30	11	44	35.04	26.20	33	5.7	172	38	-106	CMT(*)
1992	04	30	11	44	35.10	26.60	7	5.8	214	52	-47	KIR*
1992	04	30	11	44	35.10	26.60	20	6.1	172	38	-106	PPA(*)
1992	11	21	05	07	35.72	22.80	70	5.9	196	50	16	CMT(*)
1992	11	21	05	07	35.90	22.50	65	6.3	96	78	139	PPA(*)
1992	11	21	05	07	35.90	22.50	52	5.9	97	77	141	BEN*
1994	05	23	06	46	35.02	24.89	81	6.1	177	63	22	CMT(*)
1994	05	23	06	46	35.00	24.90	80	6.1	70	70	137	PPA(*)
1994	05	23	06	46	35.00	24.90	71	6.0	69	59	148	BEN*
1995	09	03	17	03	35.03	24.93	12	2.9	150	35	-11	DEL
1995	09	07	06	29	35.03	25.08	9	2.5	20	85	-150	DEL
1995	09	07	16	03	35.06	25.07	10	2.4	320	50	41	DEL
1995	09	08	00	37	35.04	25.08	9	1.8	290	90	180	DEL
1995	09	11	21	32	35.00	25.02	5	0.0	15	55	-109	DEL
1995	09	12	13	48	35.00	25.12	4	1.1	45	60	-110	DEL
1995	09	15	13	33	34.81	25.39	23	2.4	140	50	-119	DEL
1995	09	25	14	08	35.17	25.16	6	1.5	65	35	-10	DEL
1995	10	07	05	37	34.96	25.05	29	2.1	150	85	40	DEL
1995	10	08	02	53	35.25	25.24	6	1.6	55	45	-120	DEL
1995	10	14	18	30	34.89	24.86	37	1.8	190	75	-139	DEL
1995	10	15	19	23	35.26	25.07	9	1.8	140	30	-139	DEL
1995	10	20	14	09	35.16	25.17	8	2.2	70	20	0	DEL
1995	10	26	18	55	35.23	25.24	5	1.8	100	80	-30	DEL
1995	10	27	00	45	34.75	24.77	24	2.1	55	35	-70	DEL
1995	10	27	19	46	34.67	24.88	24	2.5	180	40	60	DEL
1995	10	28	19	20	35.49	25.33	18	1.1	350	45	31	DEL
1995	10	29	19	01	35.06	24.92	8	2.7	335	30	-90	DEL
1995	10	29	19	04	35.06	24.93	4	1.4	260	60	-140	DEL
1995	10	29	20	15	35.06	24.94	5	1.6	50	60	40	DEL
1995	10	31	11	29	35.15	25.14	12	1.0	60	85	90	DEL
1995	11	02	14	11	35.19	25.16	27	2.3	60	90	-180	DEL
1995	11	05	08	03	35.23	25.23	4	1.8	120	65	-11	DEL
1995	11	09	15	39	35.16	25.17	3	1.8	65	50	-40	DEL
1995	11	13	07	38	35.00	25.09	9	2.9	85	55	-100	DEL
1995	11	20	06	13	35.04	24.77	4	1.8	75	60	-110	DEL
1995	11	21	01	23	34.76	25.46	7	2.3	185	15	-60	DEL
1995	11	26	01	18	35.07	24.94	5	2.3	205	80	-20	DEL

1995	12	07	18	01	34.79	24.15	15	5.6	319	6	123	CMT
1995	12	07	20	04	35.00	25.25	5	1.9	75	30	50	DEL
1995	12	10	03	27	34.37	23.37	21	5.3	289	22	75	CMT(*)
1995	12	10	03	27	34.76	23.99	24	5.2	266	09	54	KIR*
1995	12	10	03	27	34.80	24.10	25	5.5	289	22	75	PPA(*)
1996	04	12	15	39	36.47	27.14	151	5.2	315	44	173	CMT
1996	07	20	00	00	36.07	26.92	15	6.2	196	38	-102	CMT(*)
1996	07	20	00	00	36.07	27.46	12	6.1	232	42	-52	KIR*
1996	07	20	00	00	36.15	27.10	14	6.0	195	44	-85	USG(*)
1996	07	22	01	44	36.11	26.91	15	5.0	223	36	-78	CMT
1997	09	26	08	56	35.30	23.65	13	0.2	214	67	-46	JOS
1997	09	29	18	24	35.31	23.66	14	0.0	201	83	-45	JOS
1997	10	21	05	47	35.32	23.63	15	0.0	106	76	6	JOS
1997	10	21	07	34	35.29	23.72	15	0.2	099	85	-9	JOS
1997	10	22	01	02	35.30	23.84	3	2.2	358	85	65	JOS
1997	10	28	12	44	35.34	23.68	3	0.0	194	42	-31	JOS
1997	11	05	03	18	35.39	23.71	3	0.4	42	86	15	JOS
1997	11	05	07	24	35.34	23.64	4	1.3	312	85	75	JOS
1997	11	05	12	22	34.61	23.62	40	5.4	350	34	154	CMT(*)
1997	11	05	12	22	34.51	23.93	22	5.2	309	06	108	KIR
1997	11	12	16	20	35.33	23.63	5	0.0	209	69	22	JOS
1997	11	13	01	49	35.32	23.62	4	0.6	51	87	-40	JOS
1997	11	25	13	03	35.34	23.62	4	0.0	2	65	-79	JOS
1997	11	27	15	41	35.39	23.93	12	0.0	136	71	-111	JOS
1998	10	07	18	47	34.02	25.84	22	5.1	318	60	150	CMT
1999	01	09	23	29	35.03	25.82	17	2.8	186	58	42	BEC
1999	01	11	11	19	35.02	25.94	19	2.3	205	70	40	BEC
1999	01	13	04	41	35.04	25.92	18	2.3	50	45	-10	BEC
1999	01	14	04	46	35.07	25.89	14	2.4	242	74	70	BEC
1999	01	15	07	50	35.08	26.02	18	1.9	40	40	30	BEC
1999	01	15	10	16	34.86	26.07	39	4.5	5	35	120	BEC
1999	01	19	00	37	35.07	25.87	15	2.1	55	50	0	BEC
1999	01	19	01	12	35.06	25.89	15	2.2	40	40	-50	BEC
1999	01	25	14	40	34.75	25.80	47	4.6	159	72	26	BEC
1999	01	25	14	47	34.76	25.81	44	3.5	35	50	150	BEC
1999	01	26	20	09	35.06	25.92	15	2.1	5	30	-40	BEC
1999	01	27	00	33	35.07	26.04	18	2.3	70	85	0	BEC
1999	01	28	19	00	34.81	25.81	50	3.3	40	50	140	BEC
1999	01	28	19	16	34.77	25.82	45	3.5	54	58	-42	BEC
1999	01	30	20	25	35.08	25.88	15	1.8	58	51	13	BEC
1999	01	31	05	48	35.21	26.01	16	2.8	75	70	150	BEC
1999	02	05	01	59	34.98	25.69	17	3.1	75	70	-30	BEC
1999	02	08	04	52	35.20	25.96	20	2.1	25	70	50	BEC
1999	02	10	01	08	35.07	26.11	22	2.3	85	80	60	BEC
1999	02	10	12	01	35.09	26.11	22	3.1	238	74	-70	BEC
1999	02	10	14	04	35.09	26.12	24	3.8	254	71	-66	BEC
1999	02	14	20	13	35.09	26.04	20	2.8	58	80	15	BEC
1999	02	15	11	21	35.10	26.12	22	2.2	230	80	-30	BEC
1999	02	17	00	16	35.08	26.20	29	2.7	292	75	-42	BEC
1999	02	17	17	09	34.73	25.82	41	3.3	24	58	-42	BEC
1999	02	18	16	49	34.75	25.74	42	3.4	18	76	117	BEC
1999	02	21	03	30	35.17	25.77	13	3.2	12	48	-59	BEC
1999	02	22	12	36	35.09	26.07	22	3.4	267	81	-20	BEC
1999	02	25	02	30	35.24	26.01	18	2.6	15	55	80	BEC
1999	02	26	08	41	34.94	26.12	38	2.3	36	33	-28	BEC
1999	02	26	18	10	34.95	26.10	39	2.4	340	55	-30	BEC
1999	02	27	23	50	35.05	26.11	19	3.9	40	90	175	BEC
1999	02	28	00	19	35.04	26.10	18	2.4	50	45	30	BEC
1999	03	01	03	02	35.05	26.11	22	3.6	70	71	16	BEC
1999	03	01	03	11	35.04	26.10	17	2.2	100	65	50	BEC
1999	03	01	03	28	35.04	26.12	22	3.5	240	85	-60	BEC
1999	03	01	12	18	34.94	26.10	35	3.2	90	65	-170	BEC
2000	01	27	06	51	35.52	23.51	9	4.5	205	53	-75	SED
2000	01	31	07	34	35.24	27.36	27	4.8	200	69	-54	SED

2000	02	22	11	55	34.58	25.51	12	5.2	130	79	90	SED(*)
2000	02	22	11	55	34.15	25.35	33	5.3	347	34	157	CMT(*)
2000	02	22	11	55	34.95	25.38	20	5.0	92	71	68	BEN*
2000	03	10	22	01	34.31	26.09	24	5.1	289	46	102	SED*
2000	03	10	22	01	34.13	25.98	15	5.2	256	22	72	CMT(*)
2000	03	13	14	18	35.35	23.38	36	4.7	130	63	88	SED
2000	04	05	04	36	34.22	25.85	15	5.4	301	55	120	SED*
2000	04	05	04	36	34.08	25.83	15	5.5	276	43	80	CMT(*)
2000	04	05	04	36	34.22	25.69	30	5.6	298	44	-107	USG(*)
2000	04	17	23	55	34.22	25.91	24	4.9	51	64	59	SED
2000	04	30	13	19	34.99	25.10	7	1.4	147	35	-42	MES
2000	04	30	21	15	35.00	24.70	16	2.3	233	76	69	MES
2000	05	02	18	31	34.89	24.79	32	1.2	169	55	-30	MES
2000	05	05	03	42	34.91	25.43	1	1.3	280	85	85	MES
2000	05	23	14	14	34.86	24.68	38	1.3	223	80	24	MES
2000	06	01	17	07	34.90	24.65	13	1.7	265	85	75	MES
2000	06	04	18	38	34.95	25.25	10	1.6	221	55	64	MES
2000	06	05	01	53	35.16	24.82	12	0.8	173	50	-14	MES
2000	06	11	16	27	34.99	25.10	7	1.4	315	42	-54	MES
2000	06	13	01	43	35.15	27.13	24	5.2	141	73	-162	SED(*)
2000	06	13	01	43	35.16	26.74	15	5.4	147	45	-166	CMT(*)
2000	06	13	01	43	35.17	27.16	16	5.0	49	71	-46	BEN*
2000	06	15	13	51	34.95	25.26	9	0.9	160	75	80	MES
2000	06	15	16	10	35.16	27.16	18	4.7	190	47	-91	SED
2000	06	28	08	08	34.97	25.25	10	1.4	38	68	-79	MES
2000	07	13	23	20	34.97	25.24	11	1.5	331	84	-55	MES
2000	07	17	12	12	34.47	26.58	27	4.7	323	62	-116	SED
2000	08	04	11	24	34.98	25.27	11	1.0	314	77	-69	MES
2000	08	15	16	18	34.97	25.27	10	0.9	320	88	-75	MES
2000	09	03	12	33	34.97	25.25	10	1.4	38	68	-79	MES
2000	10	04	10	51	35.04	24.57	4	2.2	143	14	-45	MES
2000	10	13	01	46	34.91	25.43	1	1.4	280	35	48	MES
2000	10	13	22	49	35.04	27.23	24	4.6	323	81	157	SED
2000	10	14	15	23	34.96	25.25	11	2.0	46	62	-66	MES
2000	10	29	19	35	34.92	24.89	32	0.6	55	78	-21	MES
2000	11	10	22	57	34.95	24.91	10	0.9	309	56	-72	MES
2000	12	03	15	44	34.95	25.56	9	1.1	160	75	80	MES
2000	12	15	05	17	34.93	24.84	35	1.4	41	83	-20	MES
2001	03	10	11	20	34.89	25.98	12	5.0	93	84	-6	SED
2001	04	01	16	16	35.01	25.02	22	0.3	129	34	-58	MES
2001	04	10	14	00	34.31	26.06	42	4.6	353	85	-169	SED
2001	04	11	08	25	34.99	23.16	24	4.6	275	48	93	SED
2001	04	27	23	31	34.91	24.80	20	3.5	142	22	-35	MES
2001	04	28	00	06	35.22	23.08	51	4.5	157	67	131	SED
2001	05	01	06	00	35.69	27.50	15	5.1	174	50	-96	SED*
2001	05	01	06	00	35.33	27.17	33	5.2	176	25	-105	CMT(*)
2001	05	04	19	51	34.62	22.77	24	4.6	64	85	22	SED
2001	06	05	15	57	34.93	25.04	15	2.4	359	26	76	MES
2001	06	09	01	28	36.19	22.98	15	4.5	349	51	-99	SED
2001	06	13	00	36	35.93	24.89	24	1.5	18	55	-37	MES
2001	06	14	17	42	35.01	24.94	26	0.8	33	84	14	MES
2001	07	14	22	14	34.97	25.15	11	1.5	14	45	-40	MES
2001	07	31	11	08	34.88	25.43	7	1.6	127	18	-56	MES
2001	07	31	23	56	34.58	24.77	15	4.2	275	71	-80	SED
2001	08	03	09	03	35.11	25.32	15	1.5	111	46	57	MES
2001	08	25	14	37	34.91	25.40	4	2.0	75	7	45	MES
2001	08	27	07	42	34.91	25.42	9	1.8	14	10	90	MES
2001	09	13	05	55	35.16	24.89	11	0.3	101	38	52	MES
2001	09	13	15	42	35.51	25.93	54	5.1	175	65	70	SED
2001	09	23	11	41	34.91	25.46	9	1.8	100	40	5	MES
2001	09	26	04	19	35.04	27.04	27	4.9	49	87	-14	SED
2001	11	04	17	23	34.06	25.43	24	5.0	90	49	71	SED
2001	11	26	04	18	34.42	24.10	15	4.5	228	4	0	MED
2001	11	26	04	21	34.79	24.06	24	4.6	311	83	-134	SED

2001	11	26	05	00	34.77	24.17	15	5.2	194	9	-27	MED
2001	11	26	05	03	34.82	24.28	42	5.1	124	72	135	SED*
2001	11	26	05	03	34.49	23.86	48	5.2	343	32	-178	CMT(*)
2001	12	21	14	25	36.00	27.48	9	4.5	328	53	-126	SED
2002	01	22	04	52	35.30	26.67	99	6.1	23	14	-161	MED(*)
2002	01	22	04	53	35.79	26.62	81	6.2	270	88	-45	SED(*)
2002	01	22	04	53	35.53	26.59	90	6.2	3	32	-178	CMT(*)
2002	01	22	04	53	35.79	26.62	84	6.2	355	30	171	USG(*)
2002	01	22	04	53	35.46	26.59	93	6.1	9	36	-176	BEN*
2002	02	24	05	32	34.81	27.28	15	4.5	340	72	-140	SED
2002	04	03	12	00	35.80	23.71	12	4.5	344	47	-96	SED(*)
2002	04	03	12	00	36.10	23.55	17	4.7	321	34	-79	MED*
2002	02	04	08	10	34.83	24.59	54	4.7	104	50	89	SED
2002	05	09	01	49	36.47	23.33	24	4.3	267	86	21	SED-
2002	05	09	01	49	36.33	23.17	17	4.6	176	21	-176	MED(*)
2002	05	21	20	53	36.34	24.41	100	5.9	260	81	179	CMT(*)
2002	05	21	20	52	36.31	24.58	125	5.8	349	74	12	MED(*)
2002	05	21	20	53	36.37	24.31	105	5.8	352	89	4	BEN*
2002	06	06	22	35	35.65	26.18	72	5.0	274	64	-91	SED(*)
2002	06	06	22	35	35.56	26.26	110	5.2	143	26	-32	CMT(*)
2002	06	06	22	35	35.30	26.56	110	5.1	140	30	-43	MED(*)
2002	06	06	22	35	35.54	26.01	94	4.9	153	31	-22	BEN*
2002	09	02	09	23	35.08	26.52	30	4.9	222	60	68	SED
2002	09	08	16	14	34.71	23.43	39	4.7	152	65	118	SED
2002	09	22	09	46	34.85	25.36	12	4.5	165	75	-156	SED
2002	10	12	05	58	34.78	26.37	33	5.0	337	89	-144	SED*
2002	10	12	05	58	34.61	25.99	15	5.4	250	29	2	CMT(*)
2003	03	01	04	06	34.72	23.94	21	4.7	27	89	-13	SED
2003	05	30	10	47	34.78	26.22	45	4.5	135	65	114	SED
2003	07	16	06	56	34.00	24.00	26	4.7	336	67	15	MED
2003	09	05	23	30	34.59	26.19	24	4.6	267	66	-37	SED
2003	10	16	22	44	36.50	23.09	24	4.3	330	54	-121	SED
2003	11	27	14	49	34.92	25.18	12	4.4	57	64	-49	SED
2004	02	07	21	17	36.04	26.91	9	5.2	355	73	-107	SED
2004	03	17	05	20	34.52	23.37	26	6.0	349	88	0	MED*
2004	03	17	05	21	34.59	23.33	24	6.1	351	88	-3	SED(*)
2004	03	18	15	14	36.08	26.48	90	4.4	234	81	-27	SED
2004	10	07	01	05	36.29	26.81	161	5.5	346	25	-167	MED

Table 1 : Overview on the entire set of fault plane solutions analysed in this study. For each event the relevant source study is given: BEC=Becker, 2000 ; BEN=Benetatos et al., 2004 ; DEC=DeChabalier et al., 1992; DEL=Delibasis et al., 1999; HAT=Hatzfeld et al., 1993a and 1993b; JOS=Jost et al., 2002; KIR=Kiratzi and Louvari, 2003; MCK=McKenzie, 1972 and 1978; PDI=Papadimitriou et al., 1993; PDO=Papadopoulos et al., 1986; PPA=Papazachos, 1973, Papazachos and Papazachou, 1997, Papazachos et al., 1991 and 2000; TAY=Taymaz et al., 1990; CMT=Harvard Centroid Moment Tensors (1977-2004); MED=INGV MEDNET (2001-2004); SED=Schweizer Erdbeben Dienst, ETH Zürich (2000-2004); USG=US Geological Survey (except CMT solutions, 1982-2002).
In case of multiple occurrences of events we selected the most reliable fault plane solution (see text) ; in the table '*' indicates the most reliable fault mechanism for the relevant event, '(*)' indicates 'similar to most reliable solution but not considered' and '–' indicates rejected fault plane solutions (those that highly deviate from the most reliable solution). No symbol is given for events that occur only once.
Note 1: In the paper by DeChaballier et al. (1992) no information is given on the event magnitude. All events from this study are shallow and were recorded by a local network on western Crete. Futhermore, none of these events was recorded by a regional network. We thus set the magnitude of these events (99 in the table) to M=2.
Note 2 : The list in the paper by Papadopoulos et al. (1986) contains no information on the hypocentral depth ; instead a subdivision into shallower ($z<60$ km) and deeper ($z>60$ km) is given. We have set the depth of the shallower category to $z=33$ km similar to the procedure applied for the global catalogues. This was also done for two events from Papazachos et al. (1991).

Table 2 :

SUBVOL.	NO.FPS	σ_1(tr)	σ_1(pl)	σ_2(tr)	σ_2(pl)	σ_3(tr)	σ_3(pl)	MISFIT	R
0	264	188	23	334	63	92	14	0.30	0.48
1	28	115	81	4	3	274	8	0.24	0.70
2	43	351	55	228	21	126	26	0.33	0.59
3	28	30	24	135	30	267	50	0.24	0.60
4	13	14	40	210	49	110	8	0.16	0.83
5	15	157	10	250	15	35	71	0.12	0.54
6	7	180	29	82	29	316	46	0.05	0.27
7	8	193	17	104	11	343	69	0.15	0.50
8	28	201	39	101	12	357	48	0.22	0.63
567	30	181	15	274	15	49	69	0.12	0.50

Table 2 : Results of stress tensor inversion for the entire data base as a whole (termed subvolume 0), for the eight subvolumes (termed subvolume 1-8) and for the sum of interplate events (termed subvolume 567). Results contain number of fault plane solutions within the relevant subvolume, directions for the three principal stresses ($\sigma_{1\text{-}3}$) in terms of trend and plunge, misfit and relative stress magnitude (R).